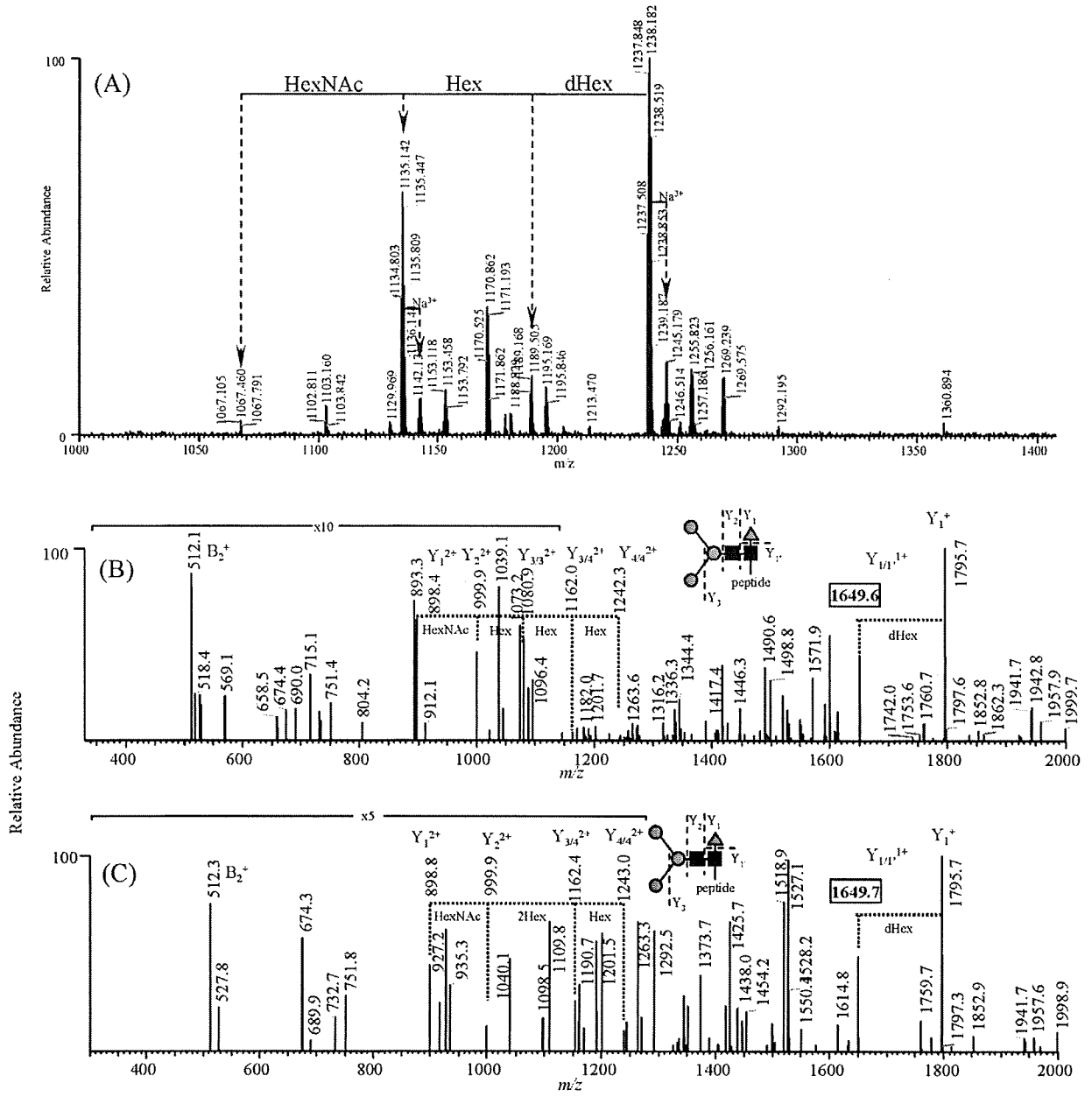

Figure 3. Integrated mass spectrum and MS/MS/MS spectra of glycopeptides 12 and 13. (A) Integrated mass spectrum of the expected Le^x-glycopeptides eluted at 41−43 min. (B) MS/MS/MS spectrum acquired from the most intense ion (*m/z* 1673.4) detected in the MS/MS spectrum of glycopeptide 12 (*m/z* 1237.8). (C) MS/MS/MS spectrum acquired from the most intense ion (*m/z* 1601.0) detected in the MS/MS spectrum of glycopeptide 13 (*m/z* 1135.4).

on the MS/MS scan was further subjected to MS/MS/MS and yielded a Y-ion series that included [peptide + 2HexNAc + 3Hex + dHex + 2H]$^{2+}$ (*m/z* 1764.3), [peptide + 2HexNAc + 2Hex + dHex+ 2H]$^{2+}$ (*m/z* 1683.5), [peptide + 2HexNAc + dHex + 2H]$^{2+}$ (*m/z* 1520.2), and [peptide + 2HexNAc + 2H]$^{2+}$ (*m/z* 1447.0). The fragment detected at *m/z* 1346.3 was assigned to our target ion, [peptide + HexNAc + 2H]$^{2+}$.

Alternative MS/MS and MS/MS/MS spectra of a Le^x-conjugated glycopeptide (glycopeptide 17) are shown in Figure 6A and B, respectively. The fragment at *m/z* 1515.4 on the MS/MS scan yielded Y-ion series that included [peptide + 2HexNAc + 3Hex + 2H]$^{2+}$ (*m/z* 1659.6), [peptide + 2HexNAc + 2Hex + 2H]$^{2+}$ (*m/z* 1578.3), and [peptide + 2HexNAc + 2H]$^{2+}$ (*m/z* 1416.5) on the MS/MS/MS scan. We deduced that the fragment at 1315.0 on the MS/MS/MS scan could be [peptide + HexNAc + 2H]$^{2+}$.

Finally we assigned out peptide + HexNAc, peptide + (dHex)HexNAc, and the peptide fragment from the product ion spectra of Le^x-conjugated glycopeptides 1−22 (Table 1). These peptide-related ions were listed as precursor ions in the second run, in which the listed ions were predominantly submitted to CID (Figure 1, second run).

Peptide Sequencing of the Expected Le^x-Conjugated Glycopeptides by the Second LC−MS/MS/MS/MS Run and Database Search Analysis. In the second run and subsequent database search analysis with modified parameters, including

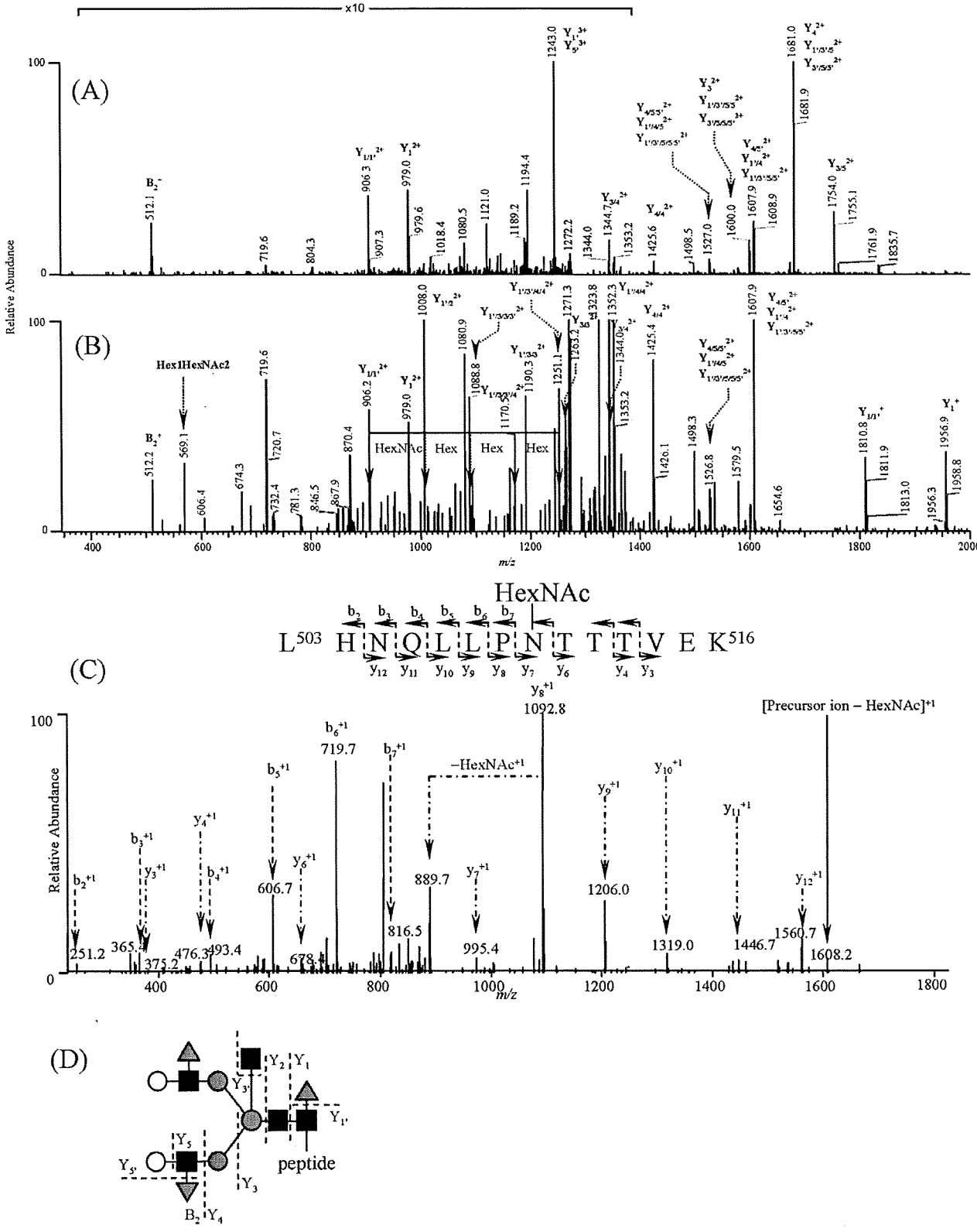

Figure 4. Identification of glycopeptide 8. (A) MS/MS spectrum acquired from the molecular ion $[M + 3H]^{3+}$ (*m/z* 1291.9) of glycopeptide 8 in Figure 2A. (B) MS/MS/MS spectrum acquired from the most intense ion (*m/z* 1681.0) in the MS/MS. (C) MS/MS/MS/MS spectrum acquired from the product ion (*m/z* 906.2) in the MS/MS/MS of glycopeptide 8, and amino acid sequence deduced from the results of database search analysis. (D) Deduced oligosaccharide structure. dHex, deoxyhexose; Hex, hexose; HexNAc, *N*-acetylhexosamine: white circle, galactose; gray circle, mannose; black square, *N*-acetylglucosamine; gray triangle, fucose.

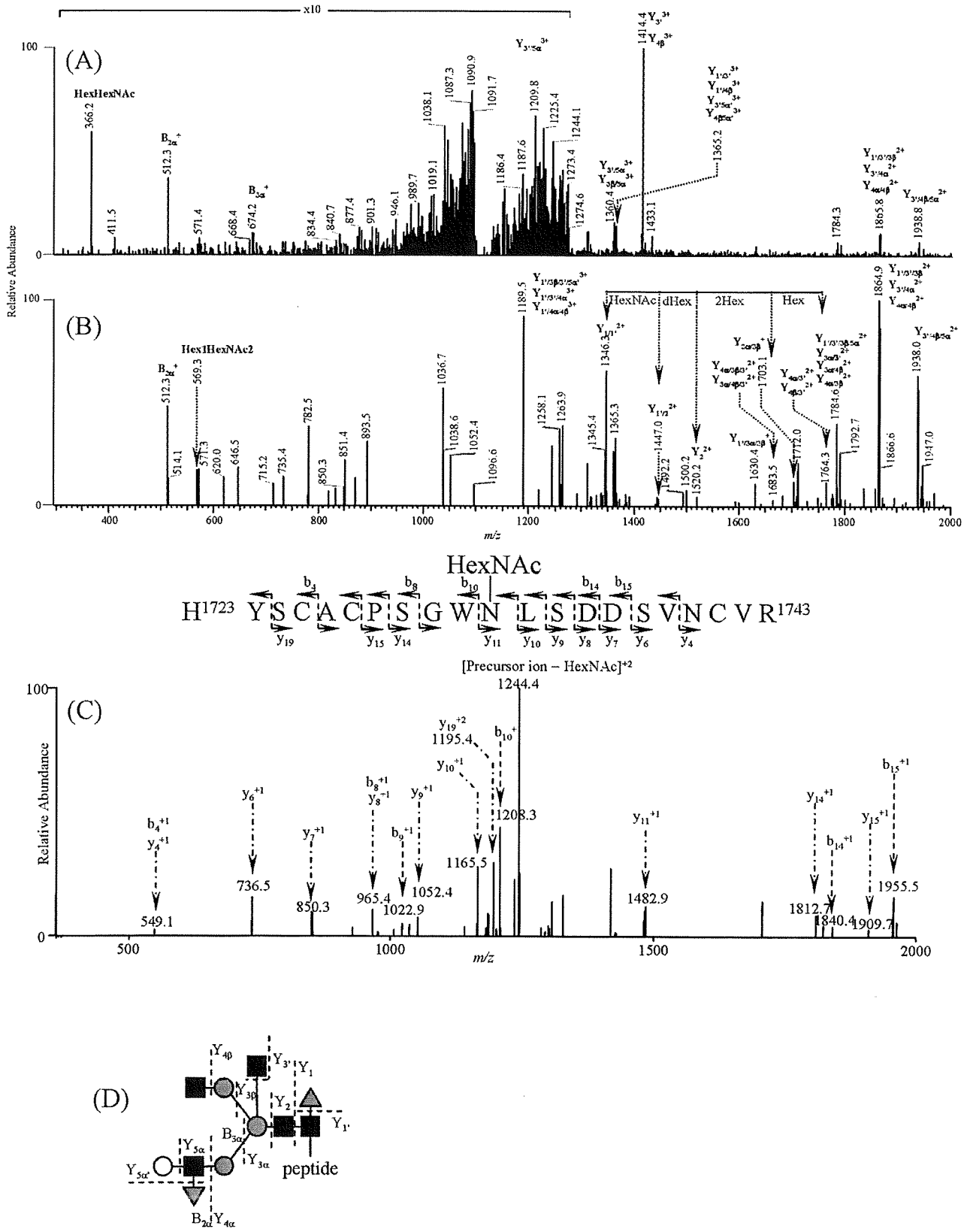

Figure 5. Identification of glycopeptide 15. (A) MS/MS spectrum acquired from the molecular ion $[M + 4H]^{4+}$ (*m/z* 1111.5) of glycopeptide 15 in Figure 2A. (B) MS/MS/MS spectrum acquired from the most intense ion (*m/z* 1414.4) in the MS/MS. (C) MS/MS/MS/MS spectrum acquired from the product ion (*m/z* 1346.3) in the MS/MS/MS of glycopeptide 15, and amino acid sequence deduced from the results of database search analysis. (D) Deduced oligosaccharide structure.

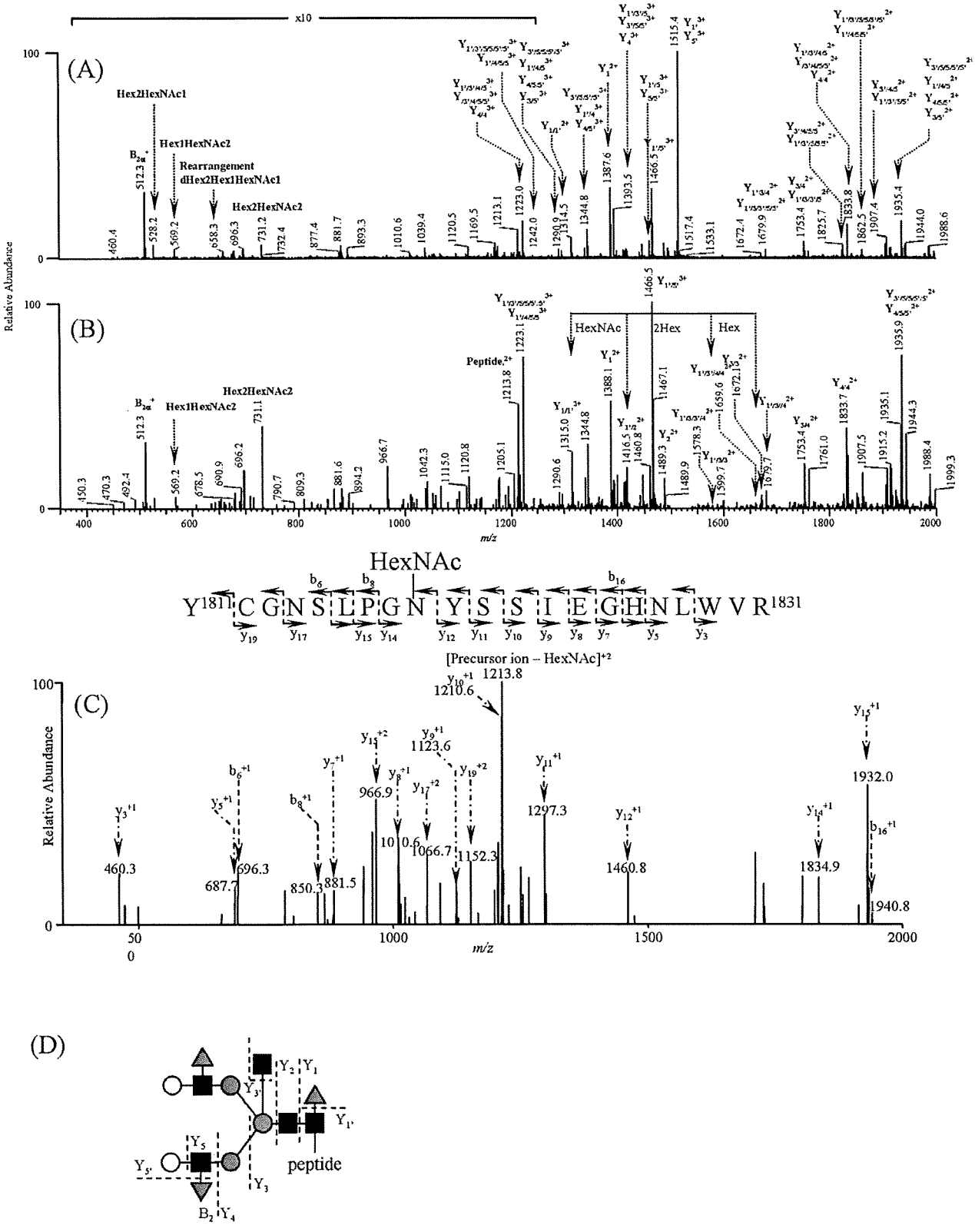

Figure 6. Identification of glycopeptide 17. (A) MS/MS spectrum acquired from the molecular ion $[M + 3H]^{3+}$ (*m/z* 1564.0) of glycopeptide 17 in Figure 2A. (B) MS/MS/MS spectrum acquired from the most intense ion (*m/z* 1515.4) in the MS/MS. (C) MS/MS/MS/MS spectrum acquired from the product ion (*m/z* 1315.0) in the MS/MS/MS of glycopeptide 17, and amino acid sequence deduced from the results of database search analysis. (D) Deduced oligosaccharide structure.

Table 1. Summary of Oligosaccharide Structures and Amino Acid Sequences of Le^x-Glycopeptides Detected by LC–MS^n and Database Search Analysis

	Candidate Le^x-glycopeptide					Peptide						Deglycosylated peptide prepared by PNGaseF-treatment					Oligosaccharide	
No.	Observed m/z value of molecular-related ion[a]	Charge state	Observed m/z value of peptide-related ion[b]	Charge state	Additional sugar residue	Amino acid sequence	Xcorr[c]	Protein identified by database search analysis	GI no.[d]	Theoretical mass[e]	Calculated mass[f]	Observed m/z value of molecular-related ion[a]	Charge state	Xcorr[c]	Theoretical mass[e]	Calculated mass[f]	Deduced Structure	Theoretical mass[g]
1	1136.129	[M+2H]^2+	673.8	2	HexNAc	E^1455GN*ATGHLMGR^1464	1.32	Cubilin precursor	88909268	1141.530	1141.530	572.280	2	2.57	1142.513	1142.545	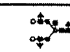	2281.845
2	1170.147	[M+3H]^3+	1448.5	1	HexNAc	N*^390LSYLAAPDIK^399	1.52	cadherin 16	6680990	1243.583	1243.564	623.291	2	3.43	1244.567	1244.567	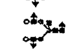	2281.845
3	1157.145	[M+3H]^3+	770.7	2	HexNAc+dHex	R^37N*WTEFLVR^45	1.33	dipeptidase 1	6651217	1189.584	1189.579	596.290	2	2.87	1190.568	1190.565	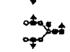	2281.845
4	1293.858	[M+3H]^3+	910.5	2	HexNAc	Y^106YN*QSAGGSHTFQR^118	1.28	H-2 class I histocompatibility antigen, K-K alpha precursor	122159	1614.718	1614.717	808.865	2	4.19	1615.702	1615.715	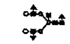	2281.845
5	1225.510	[M+3H]^3+	1613.7	1	HexNAc	T^1391WSAFQN*GTDKR^1401	1.32	low[-]density lipoprotein receptor-related protein 2 (LRP2)	124487372	1409.669	1409.673	471.227	3	1.66	1410.653	1410.659	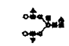	2281.845
6	1122.804	[M+3H]^3+	807.7	2	HexNAc	T^1391WSAFQN*GTDKR^1401	1.30	low[-]density lipoprotein receptor-related protein 2 (LRP2)	124187372	1409.669	1409.666	471.227	3	1.66	1410.653	1410.659	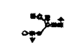	1973.735
7	1231.510	[M+3H]^3+	816.2	2	HexNAc	—[h]	—	—	—	—	—	—	—	—	—	—	—	—
8	1261.243	[M+3H]^3+	906.2	2	HexNAc	L^344HNQLLIN*TTTVEK^357	4.12	γ-glutamyltransferase 1 (γ-GTP1)	6679995	1606.868	1606.871	804.937	2	4.12	1607.852	1607.859	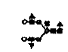	2281.845
9	1156.466	[M+5H]^5+	1070.0	3	HexNAc	^2918HHCELQN*CSSTEFTCINSRPPNRK^2943	—	low[-]density lipoprotein receptor-related protein 2 (LRP2)	124487372	3002.281	3002.269	601.663	5	4.77	3003.265	3003.279	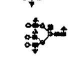	2793.035
10	1160.210	[M+4H]^4+	1120.0	2	HexNAc	S^561GQEDUYWLDVEKN*QSAK^578	1.53	alanyl (membrane) aminopeptidase	22963748700	2132.976	2132.976	—	—	—	—	—	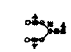	2281.845
11	1125.960	[M+5H]^5+	913.6	3	HexNAc	—	—	—	—	—	—	—	—	—	—	—	—	—
12	1237.506	[M+3H]^3+	1643.6	1	HexNAc	N*^343MSSEFYATQLR^353	1.75	γ-glutamyltransferase 1 (γ-GTP1)	6679995	1445.661	1445.660	724.340	2	3.78	1446.645	1446.665	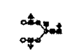	2281.845
13	1134.803	[M+3H]^3+	1649.7	1	HexNAc	N*^343MSSEFYATQLR^353	1.30	γ-glutamyltransferase 1 (γ-GTP1)	6679995	1445.661	1445.664	724.340	2	3.78	1446.645	1446.655	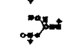	1973.735
14	1163.044	[M+4H]^4+	1295.4	2	HexNAc	V^2447VLVN*YTHKPFDIHVLHPYR^2467	1.79	low[-]density lipoprotein receptor related protein 2 (LRP2)	124487372	2384.311	2384.312	796.118	3	4.71	2385.295	2385.332	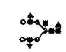	2281.845
15	1111.453	[M+4H]^4+	1340.3	2	HexNAc	H^1236YSCACPSGWN*LSDDSVNCVR^1256	2.82	low[-]density lipoprotein receptor-related protein 2 (LRP2)	124487372	2466.060	2466.059	—	—	—	—	—	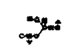	1973.735
16	1145.460	[M+4H]^4+	1187.2	2	HexNAc	—	—	—	—	—	—	—	—	—	—	—	—	—
17	1563.318	[M+3H]^3+	1315.0	2	HexNAc	Y^1343CGNSLPGN*YSSLGHNLWVR^1363	2.02	Cubilin precursor	88909268	2423.097	2423.098	—	—	—	—	—	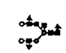	2281.845
18	1481.528	[M+2H+Na]^3+	925.1	2	HexNAc	V^106GVTDVFHN*GTQFSR^119	—	Meprin A subunit beta precursor (endopeptidase-2)	2499913	1622.805	1622.573	812.903	2	3.14	1623.789	1623.791	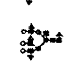	2793.035
19	1156.990	[M+4H]^4+	1282.5	2	HexNAc	—	—	—	—	—	—	—	—	—	—	—	—	—
20	1557.362	[M+3H]^3+	1204.5	2	non-substituted	N*^1783QSVVMYSVFQPLGHAHIPSK^1803	1.38	low[-]density lipoprotein receptor-related protein 2 (LRP2)	124487372	2405.259	2405.250	—	—	—	—	—	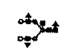	2281.845
21	1311.210	[M+H+2Na]^3+	924.9	2	HexNAc	V^106GVTDVFHN*GTQFSR^119	—	Meprin A subunit beta precursor (endopeptidase-2)	2499913	1622.805	1622.810	812.903	2	3.14	1623.789	1623.791	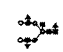	2281.845
22	1386.270	[M+3Na]^3+	948.4	2	HexNAc	V^106GVTDVFHN*GTQFSR^119	—	Meprin A subunit beta precursor (endopeptidase-2)	2499913	1622.805	1622.928	812.903	2	3.14	1623.789	1623.791	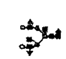	2484.925

[a] Value obtained by FTICR–MS. [b] Value obtained by IT–MS^n. [c] Value of cross correlation obtained by database search analysis. [d] GenInfo Identifier number. [e] Monoisotopic value. [f] Value calculated by subtraction of the theoretical masses of deduced oligosaccharides from the observed monoisotopic masses of the candidate Le^x-glycopeptide. [g] Monoisotoic value. [h] No data. *, modification with HexNAc; #, modification with HexNAc+dHex. Bold portions of amino acid sequences, consensus sequences of -linked oligosaccharides.

possible modification at Asn with HexNAc (203.1 u) and with dHex + HexNAc (349.1 u), seven glycopeptides were successfully sequenced with a high cross-correlation score (charge +1, Xcorr > 1.5; charge +2, Xcorr > 2.0; charge +3, Xcorr > 2.5; charge +4, Xcorr > 3.0). Figure 4C shows the MS/MS/MS/MS spectrum acquired from glycopeptide 8 (precursor ion: [peptide + HexNAc + 2H]$^{2+}$, m/z 906.2). The database search analysis resulted in Leu^{503}-Lys^{516} in γ-glutamyl transpeptidase 1 (γ-GTP1) (charge +2, Xcorr: 4.12) (Table 1). The linkage of GlcNAc at Asn^{510} in the *N*-glycosylation consensus sequence, Asn-Thr-Thr, was suggested by the good agreement between the experimental b/y-ion pattern and the predicted pattern.

The MS/MS/MS/MS spectrum acquired from [peptide + HexNAc + 2H]$^{2+}$ (m/z 1346.3, glycopeptide 15) is shown in Figure 5C. This peptide was identified as His^{1723}-Arg^{1743} in low-density lipoprotein receptor-related protein 2 (LRP2, megalin) (charge +2, Xcorr: 2.82). The b- and y-ion pattern suggested the linkage of GlcNAc at Asn^{1733} in the *N*-glycosylation consensus sequence, Asn-Lys-Ser.

Figure 6C shows the MS/MS/MS/MS spectrum acquired from another expected Le^x-conjugated glycopeptide (glycopeptide 17; precursor ion: [peptide + HexNAc + 2H]$^{2+}$, m/z 1315.0). Database search analysis revealed that this peptide could be Tyr^{1811}-Arg^{1831} in the cubilin precursor (charge +2, Xcorr: 2.02) (Table 1). It was also suggested that the linkage position of GlcNAc was Asn^{1819} in the *N*-glycosylation consensus sequence of Asn^{1819}-Tyr-Ser^{1821}.

Glycopeptides 2, 10, 12, and 14 were also successfully identified as Asn^{519}-Lys^{529} in cadherin 16 (glycosylation site: Asn^{519}; charge +1, Xcorr: 1.52), Ser^{593}-Lys^{610} in alanyl (membrane) aminopeptidase (glycosylation site: Asn^{606}; charge +2, Xcorr: 1.53), Asn^{343}-Arg^{354} in γ-GTP1 (glycosylation site: Asn^{343}; charge +1, Xcorr: 1.73) and Val^{3444}-Lys^{3463} in LRP2 (glycosylation site: Asn^{3448}; charge +2, Xcorr: 1.79), respectively. Additionally, we deduced that glycopeptides 1, 3−6, 13, and 20 could be Le^x-conjugated glycopeptides from tolerable scores (charges +1 and +2 Xcorr > 1.30) (Table 1). All identified or probable glycopeptides contained consensus sequences of *N*-linked oligosaccharides.

By the present method, three glycoproteins were identified as proteins carrying multiple Le^x-conjugated oligosaccharides—namely, γ-GTP1 (glycosylation site: Asn^{343} and Asn^{510}; glycopeptides 8, 12 and 13), LRP2 (glycosylation site: Asn^{1497}, Asn^{1676}, Asn^{1733} and Asn^{3448}; glycopeptides 5, 6, 14, 15 and 20), and a cubilin precursor (glycosylation site: Asn^{1802}, Asn^{1819}, glycopeptides 1 and 17). Only one glycopeptide was sequenced, but it was deduced that cadherin 16, dipeptidase 1, H-2 class I histocompatibility antigen, and K−K alpha precursor (H2−K(k)), and alanyl (membrane) aminopeptidase could be the Le^x-conjugated glycoproteins.

The sequences of the Le^x-conjugated glycopeptides were confirmed by an additional LC−MS/MS of deglycosylated peptides prepared by PNGaseF-treatment. Because of the deamination of Asn residues by PNGase F treatment, we set the m/z values of [peptide + nH + 0.984 u monoisotopic mass]$^{n+}$ (n = 2−5) as precursor ions on the MS/MS. By this conventional method, 8 peptides that were sequenced by our method were identified as shown in Table 1. Moreover, two peptides which could not be sequenced by our method were also identified as His^{2943}-Lys^{2966} in LRP2 (glycopeptide 9), and Val^{540}-Lys^{554} in the meprin A β subunit precursor (endopeptidase-2, glycopeptides 18, 21 and 22). On the other hand, four glycopeptides that were sequenced by our method were not identified by the conventional method. Using both methods, we failed in the sequencing of four glycopeptides.

Structural Analyses of the Oligosaccharides in the Le^x-Conjugated Glycopeptides. The carbohydrate structures of the Le^x-conjugated glycopeptides were deduced from the fragment patterns and molecular masses obtained by the first run using FTICR-MS. The structural assignment of glycopeptide 8 is shown in Figure 4A and B. The carbohydrate composition was estimated to be 3dHex 5Hex 5HexNAc from the molecular mass of the carbohydrate moiety (calculated molecular mass of the glycan moiety: 2281.850). The fragment ions at m/z 1681.0 and m/z 1425.6 in Figure 4A were assigned to Y_4^{2+} and $Y_{4/4}^{2+}$, which arose from [M + 2H]$^{2+}$ (m/z 1681.8) by the dissociation of two molecules of the Lewis-motifs. The presence of B_2^+ (m/z 512) in both Figure 4A and B also suggested the binding of two Lewis-motifs. The Y_4^{2+} further yielded [Hex + 2HexNAc]$^+$ (m/z 569.1), $Y_{1'/3/3}^{2+}$ (m/z 1190.3) and $Y_{3/3}^{2+}$ (m/z 1263.2) on the MS/MS/MS, which suggested the presence of bisecting GlcNAc. The fucosylation of reducing-end GlcNAc was proven by the detection of $Y_{1/1'}^{2+}$ ([peptide + HexNAc + 2H]$^{2+}$, m/z 906.2) and Y_1^{2+} ([peptide + dHex + HexNAc + 2H]$^{2+}$, m/z 979.0). Consequently, the glycan of glycopeptide 8 was characterized as a bisected and core-fucosylated oligosaccharide carrying two molecules of Le^x-motifs (Figure 4D). The possibility of the deduced structure was confirmed by the good agreement between the experimental mass (2281.850) and the theoretical mass (2281.845) (Table 1).

Figure 5A and B show the assignments of the carbohydrate moiety in the glycopeptide 15. The predominant ion (m/z 1414.4) in the MS/MS spectrum was assigned to [M − HexNAc + 3H]$^{3+}$ (Y_3^{3+} or $Y_{4\beta}^{3+}$). This Y_3^{3+} ($Y_{4\beta}^{3+}$) ion yielded the B_2^+ (m/z 512.3) by MS/MS/MS, suggesting the presence of only one molecule of the Lewis-motif. The presence of $Y_{1/1'}^{2+}$ (m/z 1346.3), $Y_{1'/2}^{2+}$ (m/z 1447.0) and Y_2^{2+} (m/z 1520.2) suggested the fucosylation at the reducing end of GlcNAc. The presence of bisecting GlcNAc was deduced from the detection of the ion [Hex + 2HexNAc]$^+$ (m/z 569.3) and $Y_{1'/3\alpha/3\beta}^{2+}$ (m/z 1630.4). From these fragments, the oligosaccharide structure was characterized as a bisected and core-fucosylated oligosaccharide carrying one molecule of the Le^x-motif (Figure 5D).

The deduced carbohydrate structure of glycopeptide 17 is indicated in Figure 6D. In the MS/MS spectrum, the fragments at m/z 1515.4 and m/z 1393.5 were assigned to [M − dHex + 3H]$^{3+}$ (Y_1^{3+} or Y_5^{3+}) and [M − dHex − Hex − HexNAc + 3H]$^{3+}$ (Y_4^{3+}), respectively (Figure 6A). The detection of B_2^+ (m/z 512.3) in both the MS/MS and MS/MS/MS spectra revealed the binding of two Le^x-motifs (Figure 6A and 6B). The presence of bisecting GlcNAc was suggested by the detection of the ion [Hex + 2HexNAc]$^+$ (m/z 569.2), $Y_{1'/3/3}^{2+}$ (m/z 1599.7) and $Y_{3/3}^{2+}$ (m/z 1672.1) in the MS/MS/MS spectrum (Figure 6B). The ions $Y_{1/1'}^{2+}$ ([peptide + HexNAc + 2H]$^{2+}$, m/z 1315.0) and Y_1^{2+} ([peptide + dHex + HexNAc + 2H]$^{2+}$, m/z 1388.1) revealed the fucosylation at the reducing end of GlcNAc. We also found the presence of a distinctive ion of the Lewis y (Le^y) motif, (Fucα1−2)Galβ1−4(Fucα1−3)GlcNAc, at m/z 658.3 in the MS/MS spectrum. To determine whether *N*-linked oligosaccharides contained the Le^y-motif, *N*-linked oligosaccharides were released from mouse kidney proteins and treated with α1−2 fucosidase. Then the glycan profiles of the fucosidase-treated and -untreated oligosaccharides were compared by LC/MS. No change was found in the mass spectrometric glycan profiles between the two samples, but the fragment (m/z 658) was still detected in the MS/MS spectra of the enzyme-treated

glycopeptide 17 (data not shown). These results suggest the absence of α1−2 fucose on the glycopeptides. Consequently, we assigned the glycans of glycopeptide 17 to a bisected and core-fucosylated oligosaccharide carrying two Le^x-motifs (Figure 6D).

The oligosaccharide structures of other Le^x-conjugated glycopeptides were deduced from their B- and Y-type ions as well as the molecular masses obtained by FTICR−MS in the same manner (Table 1 and Figure 7). The most common structure was a bisected and fucosylated complex-type biantennary oligosaccharide carrying two Le^x-motifs (glycopeptides 1−5, 8, 10, 12, 14, 17, 20 and 21). A bisected and core-fucosylated complex-type biantennary oligosaccharide carrying one Le^x-motif was found in glycopeptides 6, 13, and 15. A bisected and core-fucosylated complex-type triantennary oligosaccharide carrying three Le^x-motifs was found in glycopeptides 9 and 18. The oligosaccharide structure of the glycopeptide in glycopeptide 22 was a triantennary carrying two Le^x-motifs. All experimental molecular masses of the deduced glycopeptides were identical to their theoretical masses (Table 1).

Discussion

Several glycan-epitopes, including Lewis antigens, HNK-1, and polysialic acid, have been widely shown to be involved in the physiological functions of glycoproteins and certain diseases. Some oligosaccharide-related antigens are being used as diagnostic markers of tumors in a clinical stage.[42,43] However, only a few proteins are known to carry the glycan-epitopes. To understand the physiological roles of the glycan-epitopes and to develop more effective diagnostic markers, we need methods that allow for the identification of target proteins carrying the glycan motif of interest. Glycan-epitopes are often detected by two-dimensional (2D)-electrophoresis in combination with lectin or immuno-blotting. The stained spots are subjected to in-gel tryptic digestion followed by protein identification by MS/MS and database search analysis. There are still problems in this procedure with the verification of the glycan structure in the identified protein. In addition, the procedure cannot be employed on hydrophobic membrane proteins having a high molecular weight.

In the present study, all proteins in the mouse kidney were digested into peptides, and the fucosylated glycopeptides were enriched by lectin-affinity chromatography. The resulting fucosylated glycopeptides were subjected to two different runs of LC−MS^n. In the first run, the elution positions of Le^x-conjugated glycopeptides in the tryptic peptide map were located based on the presence of Le^x-motif-distinctive ions. We picked out the product ion spectra of expected Le^x-conjugated glycopeptides from the elution positions and carefully assigned the peptide + HexNAc, peptide + (dHex)HexNAc, and peptide fragment. Then the fucosylated glycopeptides were subjected to a second run in which the peptide-related ions were set as precursor ions. We successfully identified γ-GTP1, LRP2, and the cubilin precursor as Le^x-conjugated glycoproteins by sequencing of 2−5 glycopeptides. Although only one glycopeptide was sequenced, cadherin 16, dipeptidase I, H2−K(k) and alanyl (membrane) aminopeptidase were characterized as Le^x-conjugated glycoproteins based on the good agreement between the experimental and theoretical masses of glycopeptides and their fragment patterns. Some of these were membrane proteins with high molecular masses over 400 kDa, the identification of which might have been difficult by 2D-electrophoresis with Western blotting.

Carbohydrate structures of the identified glycopeptides were deduced from the accurate molecular masses as well as fragment patterns obtained by the first run. We confirmed that all glycopeptides contained a bisected and core-fucosylated oligosaccharide carrying one or two molecules of Le^x-motifs at the *N*-linked oligosaccharide consensus sequence. Our model tissue was a mouse kidney in which we had previously confirmed the presence of Lewis x [Galβ1−4(Fucα1−3)GlcNAc] and/or y [(Fucα1−2)Galβ1−4(Fucα1−3)GlcNAc] motifs as well as the absence of Lewis a [Galβ1−3(Fucα1−4)GlcNAc] or b [(Fucα1−2)Galβ1−3(Fucα1−4)GlcNAc] motifs.[39] In this study, the Le^y-distinctive ions, (2dHex + Hex + HexNAc)$^+$ (*m*/*z* 658), were found in all MS/MS spectra of Lewis-conjugated peptides. However, treatment of α 1−2 fucosidase led to no change in the mass spectrometric glycan profile, suggesting the absence of the Le^y-motif. Recently, several groups have reported the internal migration of fucose residues in the ESI−CID of underived or derived carbohydrates.[44−48] Fucose residues are transferred between branches in liberated *N*-linked oligosaccharides by the ESI−CID.[49] Our finding suggests that the rearrangement of fucose residues also occurs by the ESI−CID of glycopeptides. This phenomenon makes it difficult to deduce the oligosaccharide structure from only the fragmentation pattern. A simultaneous use of lectins and/or antibodies would be crucial for the identification of the desired glycoproteins.

γ-Glutamyl transpeptidase 1 is associated with glutathione salvage, metabolism of endogenous mediators such as leukotrienes and prostaglandins. The attachment of Le^x-conjugated oligosaccharide to mouse γ-GTP 1 has already been demonstrated by Yamashita et al.[51] They determined the carbohydrate structures by the purification of γ-GTP 1 and the sequential exoglycosidase digestion in combination with methylation analysis. The oligosaccharide structures deduced from the MS/MS and MS/MS/MS spectra were in good agreement with those they reported. Furthermore, we revealed the heterogeneity of glycosylation on Asn^{343}.

Dipeptidase 1 is a glycosylphosphatidylinositol-anchored membrane glycoprotein. This protein is highly expressed in the kidney and small intestine and plays an important role in the degradation of cysteinyl-glycine, a glutathione produced by the removal of the glutamyl group from γ-glutamyl cysteinyl-glycine by γ-GTP.[52] The present study is the first report on the oligosaccharide structures of a mouse renal dipeptidase.

Cubilin, which is highly expressed in the renal proximal tubules, is a 460 kDa membrane glycoprotein consisting of 27 CUB (complement components C1r/C1s, Uegf, and bone morphogenic protein-1) domains. Cubilin is an endocytic receptor for intrinsic factor vitamin B12, albumin, apolipoprotein A-I, receptor-associated protein, immune globulin light chain and high-density lipoprotein.[50] These factors bind to cubilin through their CUB domains. The Le^x-conjugated oligosaccharides we found were all located on Asn^{1802} and Asn^{1819} in the CUB12 domain (Figure 8).

Low-density lipoprotein receptor-related protein 2, a high molecular weight membrane protein (520 kDa), is an endocytic receptor for several ligands, vitamin-binding proteins, apolipoproteins, hormones and enzymes. Cubilin and LRP2 are coexpressed in the renal proximal tubules and are associated with tubular protein reabsorption, vitamin metabolism and calcium homeostasis. Low-density lipoprotein receptor-related protein 2 consists of four ligand-binding sites containing cysteine-rich complement-type repeats and epidermal growth

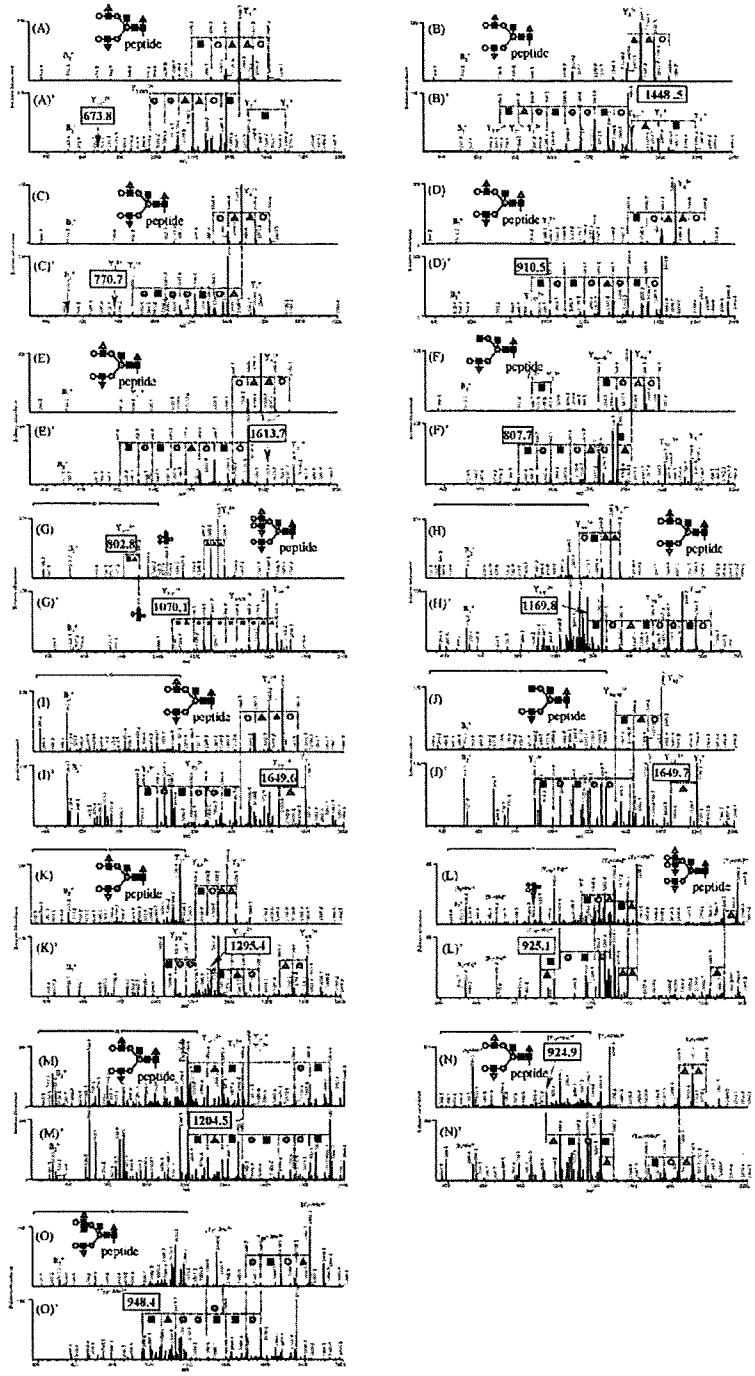

Figure 7. MS/MS and the MS/MS/MS spectra of glycopeptides 1−6, 9, 10, 12−14, 18 and 20−22, and deduced oligosaccharide structures. Boxed values are peptide-related ions. (A) MS/MS spectrum of the molecular ion (*m/z* 1136.4) of glycopeptide 1. (A′) MS/MS/MS spectrum of the predominant ion (*m/z* 1448.2) of (A). (B) MS/MS spectrum of glycopeptide 2 (*m/z* 1170.8). (B′) MS/MS/MS spectrum of the ion (*m/z* 1499.3) in (B). (C) MS/MS spectrum of glycopeptide 3(*m/z* 1152.5). (C′) MS/MS/MS spectrum of the ion (*m/z* 1472.5) in (C). (D) MS/MS spectrum of glycopeptide 4 (*m/z* 1294.2). (D′) MS/MS/MS spectrum of the ion (*m/z* 1685.0) in (D). (E) MS/MS spectrum of glycopeptide 5 (*m/z* 1226.0). (E′) MS/MS/MS spectrum of the ion (*m/z* 1582.6) in (E). (F) MS/MS spectrum of glycopeptide 6(*m/z* 1123.4). (F′) MS/MS/MS spectrum of the ion (*m/z* 1428.4) in (F). (G) MS/MS spectrum of glycopeptide 9 (*m/z* 1156.9). (G′) MS/MS/MS spectrum of the ion (*m/z* 1318.5) in (G). (H) MS/MS spectrum of glycopeptide 10 (*m/z* 1100.8). (H′) MS/MS/MS spectrum of the ion (*m/z* 1297.1) in (H). (I) MS/MS spectrum of glycopeptide 12 (*m/z* 1238.1). (I′) MS/MS/MS spectrum of the ion (*m/z* 1673.6) in (I). (J) MS/MS spectrum of glycopeptide 13 (*m/z* 1135.5). (J′) MS/MS/MS spectrum of the ion (*m/z* 1600.3) in (J). (K) MS/MS spectrum of glycopeptide 14 (*m/z* 1163.5). (K′) MS/MS/MS spectrum of the predominant ion (*m/z* 1380.8) in (K). (L) MS/MS spectrum of glycopeptide 18 (*m/z* 1482.6). (L′) MS/MS/MS spectrum of the predominant ion (*m/z* 1433.9) in (L). (M) MS/MS spectrum of glycopeptide 20 (*m/z* 1558.1). (M′) MS/MS/MS spectrum of the predominant ion (*m/z* 1509.8) in (M). (N) MS/MS spectrum of glycopeptide 21 (*m/z* 1279.2). (N′) MS/MS/MS spectrum of the predominant ion (*m/z* 1263.5) in (N). (O) MS/MS spectrum of glycopeptide 22 (*m/z* 1387.5). (O′) MS/MS/MS spectrum of the predominant ion (*m/z* 1825.5) in (O). White circle, galactose; gray circle, mannose; black square, *N*-acetylglucosamine; gray triangle, fucose.

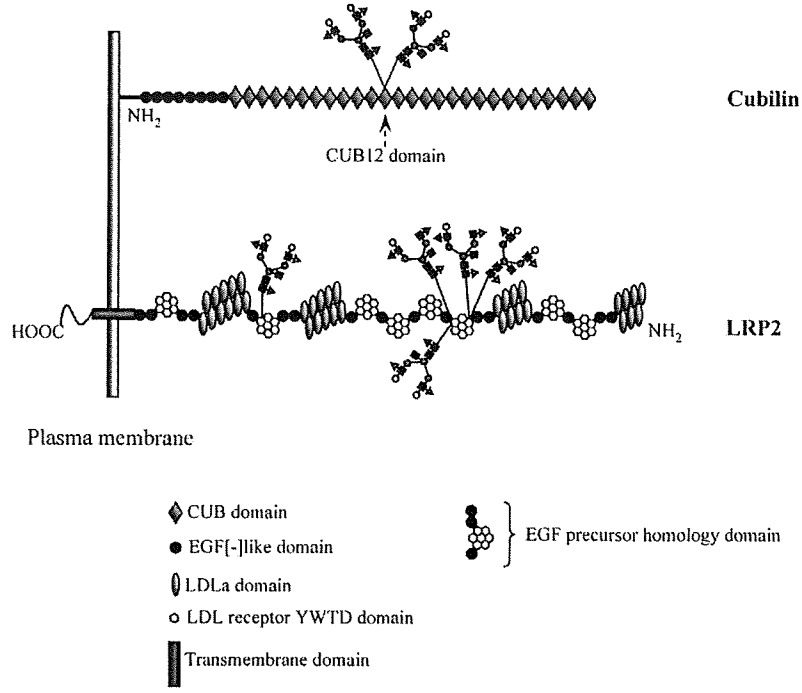

Figure 8. Location of Le^x-conjugated oligosaccharides on cubilin and LRP2. CUB, C1r/C1s, Uegf, and bone morphogenic protein-1; LDLa, Low-density lipoprotein receptor domain class A.

factor (EGF) precursor homology domains, which are associated with pH-dependent ligand dissociation. A previous study demonstrated the linkage of high-mannose-type and bi- and triantennary complex-type oligosaccharides bearing core fucose and bisecting GlcNAc. But there have been no reports on the presence of Le^x-conjugated oligosaccharides in rat kidney LRP2.[53] Interestingly, all of the Le^x-conjugated oligosaccharides we found were located in the EGF precursor homology domains (Asn^{1497}, Asn^{1676}, Asn^{1733} and Asn^{3448}). Furthermore, heterogeneity of glycosylation on Asn^{1497} was observed (Figure 8).

The cadherin 16, H2−K(k) protein and alanyl (membrane) aminopeptidase (aminopeptidase N) were also identified as Le^x-conjugated glycoproteins. Cadherin 16 is a kidney-specific cadherin that is associated with Ca^{2+}-dependent cell−cell adhesion.[54] The H2−K(k) protein, which is a mouse-specific histocompatibility antigen (H-2 antigen), is involved in the presentation of foreign antigens to the immune system. Alanyl (membrane) aminopeptidase (aminopeptidase N) is a transmembrane protein that is expressed predominantly in intestinal mucosa and kidney tissue.[55,56] It was reported that this enzyme is involved in several biological events such as tumorigenesis and immune system.[57] These proteins were unknown to be Le^x-conjugated proteins.

Using the present method, we successfully identified 14 Le^x-conjugated glycopeptides (12 peptides). Some peptides were found to be glycosylated with different Le^x-conjugated oligosaccharides (glycopeptides 5 and 6; glycopeptides 12 and 13). In most cases only a peptide carrying a major oligosaccharide was identified as a Le^x-conjugated glycopeptide. Minor Le^x-conjugated glycopeptides were not subjected to MS/MS/MS in the first run because they were less intense. Such minor glycopeptides might be identified by an additional run in which the glycopeptides identified in the first run are excluded. In addition, our method tended to fail in the identification of glycopeptides having high molecular mass (>4500 Da), glycopeptides detected as triply charged ions, and glycopeptides containing triantennary oligosaccharides. These glycopeptides yielded a smaller number of peptide-related ions, which was insufficient for further CID, and database search analysis resulted in false-positive proteins, for example, a peptide not containing *N*-glycan consensus sequences. Using a conventional approach that included LC−MS/MS of the PNGase F-treated tryptic digest, we found two additional Le^x-expected peptides. One was a high molecular mass peptide (3002 Da) containing a triantennary oligosaccharide, and the other was a peptide detected as sodium adducts in our method. The conventional approach has the advantage of peptide sequencing, but does not allow confirmation of the Lewis-motif in the oligosaccharide. Unlike the classical glycomic approaches that are used for the comprehensive analysis of glycopeptides, our method focused only on Lewis-conjugated glycopeptides. Accordingly, it could be applicable to the identification and screening of glycoproteins carrying target glycan-motifs.

Acknowledgment. This study was supported in part by a Grant-in-Aid from the Ministry of Health, Labor, and Welfare, by the Core Research for the Evolutional Science and Technology Program (CREST), and by the Japan Science and Technology Corp (JST).

References

(1) Dwek, R. A. Glycobiology: Toward Understanding the Function of Sugars. *Chem. Rev.* **1996**, *96*, 683–720.
(2) Helenius, A.; Aebi, M. Intracellular functions of N-linked glycans. *Science* **2001**, *291*, 2364–2369.
(3) Zak, I.; Lewandowska, E.; Gnyp, W. Selectin glycoprotein ligands. *Acta Biochim. Pol.* **2000**, *47*, 393–412.
(4) Feizi, T.; Gooi, H. C.; Childs, R. A.; Picard, J. K.; Uemura, K.; Loomes, L. M.; Thorpe, S. J.; Hounsell, E. F. Tumour-associated and differentiation antigens on the carbohydrate moieties of mucin-type glycoproteins. *Biochem. Soc. Trans.* **1984**, *12*, 591–596.

(5) Kannagi, R.; Izawa, M.; Koike, T.; Miyazaki, K.; Kimura, N. Carbohydrate-mediated cell adhesion in cancer metastasis and angiogenesis. *Cancer Sci.* **2004**, *95*, 377–384.
(6) Hada, T.; Kondo, M.; Yasukawa, K.; Amuro, Y.; Higashino, K. Discrimination of liver cirrhosis from chronic hepatitis by measuring the ratio of Aleuria aurantia lectin-reactive serum cholinesterase to immunoreactive protein. *Clin. Chim. Acta* **1999**, *281*, 37–46.
(7) Sutton-Smith, M.; Morris, H. R.; Grewal, P. K.; Hewitt, J. E.; Bittner, R. E.; Goldin, E.; Schiffmann, R.; Dell, A. MS screening strategies: investigating the glycomes of knockout and myodystrophic mice and leukodystrophic human brains. *Biochem. Soc. Symp.* **2002**, 105–115.
(8) Taniguchi, N.; Ekuni, A.; Ko, J. H.; Miyoshi, E.; Ikeda, Y.; Ihara, Y.; Nishikawa, A.; Honke, K.; Takahashi, M. A glycomic approach to the identification and characterization of glycoprotein function in cells transfected with glycosyltransferase genes. *Proteomics* **2001**, *1*, 239–247.
(9) Morelle, W.; Michalski, J. C. Glycomics and mass spectrometry. *Curr. Pharm. Des.* **2005**, *11*, 2615–2645.
(10) Morelle, W.; Canis, K.; Chirat, F.; Faid, V.; Michalski, J. C. The use of mass spectrometry for the proteomic analysis of glycosylation. *Proteomics* **2006**, *6*, 3993–4015.
(11) Hagglund, P.; Matthiesen, R.; Elortza, F.; Hojrup, P.; Roepstorff, P.; Jensen, O. N.; Bunkenborg, J. An enzymatic deglycosylation scheme enabling identification of core fucosylated N-glycans and O-glycosylation site mapping of human plasma proteins. *J. Proteome Res.* **2007**, *6*, 3021–3031.
(12) Alvarez-Manilla, G.; Atwood, J., 3rd; Guo, Y.; Warren, N. L.; Orlando, R.; Pierce, M. Tools for glycoproteomic analysis: size exclusion chromatography facilitates identification of tryptic glycopeptides with N-linked glycosylation sites. *J. Proteome Res.* **2006**, *5*, 701–708.
(13) Zhao, J.; Qiu, W.; Simeone, D. M.; Lubman, D. M. N-linked glycosylation profiling of pancreatic cancer serum using capillary liquid phase separation coupled with mass spectrometric analysis. *J. Proteomé Res.* **2007**, *6*, 1126–1138.
(14) Kyselova, Z.; Mechref, Y.; Al Bataineh, M. M.; Dobrolecki, L. E.; Hickey, R. J.; Vinson, J.; Sweeney, C. J.; Novotny, M. V. Alterations in the serum glycome due to metastatic prostate cancer. *J. Proteome Res.* **2007**, *6*, 1822–1832.
(15) Zamfir, A.; Seidler, D. G.; Schonherr, E.; Kresse, H.; Peter-Katalinic, J. On-line sheathless capillary electrophoresis/nanoelectrospray ionization-tandem mass spectrometry for the analysis of glycosaminoglycan oligosaccharides. *Electrophoresis* **2004**, *25*, 2010–2016.
(16) Karlsson, N. G.; Wilson, N. L.; Wirth, H. J.; Dawes, P.; Joshi, H.; Packer, N. H. Negative ion graphitised carbon nano-liquid chromatography/mass spectrometry increases sensitivity for glycoprotein oligosaccharide analysis. *Rapid Commun. Mass Spectrom.* **2004**, *18*, 2282–2292.
(17) Kawasaki, N.; Ohta, M.; Itoh, S.; Hyuga, M.; Hyuga, S.; Hayakawa, T. Usefulness of sugar mapping by liquid chromatography/mass spectrometry in comparability assessments of glycoprotein products. *Biologicals* **2002**, *30*, 113–123.
(18) Kremmer, T.; Szollosi, E.; Boldizsar, M.; Vincze, B.; Ludanyi, K.; Imre, T.; Schlosser, G.; Vekey, K. Liquid chromatographic and mass spectrometric analysis of human serum acid alpha-1-glycoprotein. *Biomed. Chromatogr.* **2004**, *18*, 323–329.
(19) Thomsson, K. A.; Karlsson, H.; Hansson, G. C. Sequencing of sulfated oligosaccharides from mucins by liquid chromatography and electrospray ionization tandem mass spectrometry. *Anal. Chem.* **2000**, *72*, 4543–4549.
(20) Kawasaki, N.; Ohta, M.; Hyuga, S.; Hyuga, M.; Hayakawa, T. Application of liquid chromatography/mass spectrometry and liquid chromatography with tandem mass spectrometry to the analysis of the site-specific carbohydrate heterogeneity in erythropoietin. *Anal. Biochem.* **2000**, *285*, 82–91.
(21) Schmid, D.; Behnke, B.; Metzger, J.; Kuhn, R. Nano-HPLC-mass spectrometry and MEKC for the analysis of oligosaccharides from human milk. *Biomed. Chromatogr.* **2002**, *16*, 151–156.
(22) Maslen, S.; Sadowski, P.; Adam, A.; Lilley, K.; Stephens, E. Differentiation of isomeric N-glycan structures by normal-phase liquid chromatography-MALDI-TOF/TOF tandem mass spectrometry. *Anal. Chem.* **2006**, *78*, 8491–8498.
(23) Yuan, J.; Hashii, N.; Kawasaki, N.; Itoh, S.; Kawanishi, T.; Hayakawa, T. Isotope tag method for quantitative analysis of carbohydrates by liquid chromatography-mass spectrometry. *J. Chromatogr. A* **2005**, *1067*, 145–152.
(24) Lawrence, R.; Olson, S. K.; Steele, R. E.; Wang, L.; Warrior, R.; Cummings, R. D.; Esko, J. D. Evolutionary differences in glycosaminoglycan fine structure detected by quantitative glycan reductive isotope labeling. *J. Biol. Chem.* **2008**, *283*, 33674–33684.
(25) Ridlova, G.; Mortimer, J. C.; Maslen, S. L.; Dupree, P.; Stephens, E. Oligosaccharide relative quantitation using isotope tagging and normal-phase liquid chromatography/mass spectrometry. *Rapid Commun. Mass Spectrom.* **2008**, *22*, 2723–2730.
(26) Harazono, A.; Kawasaki, N.; Kawanishi, T.; Hayakawa, T. Site-specific glycosylation analysis of human apolipoprotein B100 using LC/ESI MS/MS. *Glycobiology* **2005**, *15*, 447–462.
(27) Itoh, S.; Kawasaki, N.; Harazono, A.; Hashii, N.; Matsuishi, Y.; Kawanishi, T.; Hayakawa, T. Characterization of a gel-separated unknown glycoprotein by liquid chromatography/multistage tandem mass spectrometry: analysis of rat brain Thy-1 separated by sodium dodecyl sulfate-polyacrylamide gel electrophoresis. *J. Chromatogr. A* **2005**, *1094*, 105–117.
(28) Satomi, Y.; Shimonishi, Y.; Hase, T.; Takao, T. Site-specific carbohydrate profiling of human transferrin by nano-flow liquid chromatography/electrospray ionization mass spectrometry. *Rapid Commun. Mass Spectrom.* **2004**, *18*, 2983–2988.
(29) Wuhrer, M.; Catalina, M. I.; Deelder, A. M.; Hokke, C. H. Glycoproteomics based on tandem mass spectrometry of glycopeptides. *J. Chromatogr., B: Analyt. Technol. Biomed. Life Sci.* **2007**, *849*, 115–128.
(30) Stadlmann, J.; Pabst, M.; Kolarich, D.; Kunert, R.; Altmann, F. Analysis of immunoglobulin glycosylation by LC-ESI-MS of glycopeptides and oligosaccharides. *Proteomics* **2008**, *8*, 2858–2871.
(31) Picariello, G.; Ferranti, P.; Mamone, G.; Roepstorff, P.; Addeo, F. Identification of N-linked glycoproteins in human milk by hydrophilic interaction liquid chromatography and mass spectrometry. *Proteomics* **2008**, *8*, 3833–3847.
(32) Hirabayashi, J. Lectin-based structural glycomics: glycoproteomics and glycan profiling. *Glycoconj. J.* **2004**, *21*, 35–40.
(33) Taketa, K. Characterization of sugar chain structures of human alpha-fetoprotein by lectin affinity electrophoresis. ibarahp@oka.urban.ne.jp. *Electrophoresis* **1998**, *19*, 2595–2602.
(34) Kuno, A.; Kato, Y.; Matsuda, A.; Kaneko, M. K.; Ito, H.; Amano, K.; Chiba, Y.; Narimatsu, H.; Hirabayashi, J. Focused Differential Glycan Analysis with the Platform Antibody-assisted Lectin Profiling for Glycan-related Biomarker Verification. *Mol. Cell. Proteomics* **2009**, *8*, 99–108.
(35) Madera, M.; Mechref, Y.; Klouckova, I.; Novotny, M. V. Semiautomated high-sensitivity profiling of human blood serum glycoproteins through lectin preconcentration and multidimensional chromatography/tandem mass spectrometry. *J. Proteome Res.* **2006**, *5*, 2348–2363.
(36) Yang, Z.; Hancock, W. S.; Chew, T. R.; Bonilla, L. A study of glycoproteins in human serum and plasma reference standards (HUPO) using multilectin affinity chromatography coupled with RPLC-MS/MS. *Proteomics* **2005**, *5*, 3353–3366.
(37) Zhao, J.; Simeone, D. M.; Heidt, D.; Anderson, M. A.; Lubman, D. M. Comparative serum glycoproteomics using lectin selected sialic acid glycoproteins with mass spectrometric analysis: application to pancreatic cancer serum. *J. Proteome Res.* **2006**, *5*, 1792–1802.
(38) Hashii, N.; Kawasaki, N.; Itoh, S.; Hyuga, M.; Kawanishi, T.; Hayakawa, T. Glycomic/glycoproteomic analysis by liquid chromatography/mass spectrometry: analysis of glycan structural alteration in cells. *Proteomics* **2005**, *5*, 4665–4672.
(39) Hashii, N.; Kawasaki, N.; Itoh, S.; Harazono, A.; Matsuishi, Y.; Hayakawa, T.; Kawanishi, T. Specific detection of Lewis x-carbohydrates in biological samples using liquid chromatography/multiple-stage tandem mass spectrometry. *Rapid Commun. Mass Spectrom.* **2005**, *19*, 3315–3321.
(40) Carr, S. A.; Huddleston, M. J.; Bean, M. F. Selective identification and differentiation of N- and O-linked oligosaccharides in glycoproteins by liquid chromatography-mass spectrometry. *Protein Sci.* **1993**, *2*, 183–196.
(41) Harazono, A.; Kawasaki, N.; Itoh, S.; Hashii, N.; Ishii-Watabe, A.; Kawanishi, T.; Hayakawa, T. Site-specific N-glycosylation analysis of human plasma ceruloplasmin using liquid chromatography with electrospray ionization tandem mass spectrometry. *Anal. Biochem.* **2006**, *348*, 259–268.
(42) Ueda, T.; Shimada, E.; Urakawa, T. The clinicopathologic features of serum CA 19−9-positive colorectal cancers. *Surg. Today* **1994**, *24*, 518–525.
(43) Nakagoe, T.; Sawai, T.; Tsuji, T.; Jibiki, M.; Ohbatake, M.; Nanashima, A.; Yamaguchi, H.; Yasutake, T.; Ayabe, H.; Tagawa, Y. Differences in release mechanisms and distributions for sialyl Le(a) and sialyl Le(x) antigens in colorectal cancer. *Ann. Surg. Oncol.* **2000**, *7*, 289–295.

(44) Harvey, D. J.; Mattu, T. S.; Wormald, M. R.; Royle, L.; Dwek, R. A.; Rudd, P. M. "Internal residue loss": rearrangements occurring during the fragmentation of carbohydrates derivatized at the reducing terminus. *Anal. Chem.* **2002**, *74*, 734–740.

(45) Mattu, T. S.; Royle, L.; Langridge, J.; Wormald, M. R.; Van den Steen, P. E.; Van Damme, J.; Opdenakker, G.; Harvey, D. J.; Dwek, R. A.; Rudd, P. M. O-glycan analysis of natural human neutrophil gelatinase B using a combination of normal phase-HPLC and online tandem mass spectrometry: implications for the domain organization of the enzyme. *Biochemistry* **2000**, *39*, 15695–15704.

(46) Brull, L. P.; Kovacik, V.; Thomas-Oates, J. E.; Heerma, W.; Haverkamp, J. Sodium-cationized oligosaccharides do not appear to undergo 'internal residue loss' rearrangement processes on tandem mass spectrometry. *Rapid Commun. Mass Spectrom.* **1998**, *12*, 1520–1532.

(47) Franz, A. H.; Lebrilla, C. B. Evidence for long-range glycosyl transfer reactions in the gas phase. *J. Am. Soc. Mass Spectrom.* **2002**, *13*, 325–337.

(48) Ma, Y. L.; Vedernikova, I.; Van den Heuvel, H.; Claeys, M. Internal glucose residue loss in protonated O-diglycosyl flavonoids upon low-energy collision-induced dissociation. *J. Am. Soc. Mass Spectrom.* **2000**, *11*, 136–144.

(49) Wuhrer, M.; Koeleman, C. A.; Hokke, C. H.; Deelder, A. M. Mass spectrometry of proton adducts of fucosylated N-glycans: fucose transfer between antennae gives rise to misleading fragments. *Rapid Commun. Mass Spectrom.* **2006**, *20*, 1747–1754.

(50) Christensen, E. I.; Birn, H. Megalin and cubilin: synergistic endocytic receptors in renal proximal tubule. *Am. J. Physiol. Renal Physiol.* **2001**, *280*, F562–573.

(51) Yamashita, K.; Hitoi, A.; Tateishi, N.; Higashi, T.; Sakamoto, Y.; Kobata, A. The structures of the carbohydrate moieties of mouse kidney gamma-glutamyltranspeptidase: occurrence of X-antigenic determinants and bisecting N-acetylglucosamine residues. *Arch. Biochem. Biophys.* **1985**, *240*, 573–582.

(52) Habib, G. M.; Shi, Z. Z.; Cuevas, A. A.; Lieberman, M. W. Identification of two additional members of the membrane-bound dipeptidase family. *Faseb J.* **2003**, *17*, 1313–1315.

(53) Morelle, W.; Haslam, S. M.; Ziak, M.; Roth, J.; Morris, H. R.; Dell, A. Characterization of the N-linked oligosaccharides of megalin (gp330) from rat kidney. *Glycobiology* **2000**, *10*, 295–304.

(54) Wendeler, M. W.; Praus, M.; Jung, R.; Hecking, M.; Metzig, C.; Gessner, R. Ksp-cadherin is a functional cell-cell adhesion molecule related to LI-cadherin. *Exp. Cell Res.* **2004**, *294*, 345–355.

(55) Barnes, K.; Walkden, B. J.; Wilkinson, T. C.; Turner, A. J. Expression of endothelin-converting enzyme in both neuroblastoma and glial cell lines and its localization in rat hippocampus. *J. Neurochem.* **1997**, *68*, 570–577.

(56) Lucius, R.; Sievers, J.; Mentlein, R. Enkephalin metabolism by microglial aminopeptidase N (CD13). *J. Neurochem.* **1995**, *64*, 1841–1847.

(57) Luan, Y.; Xu, W. The structure and main functions of aminopeptidase N. *Curr. Med. Chem.* **2007**, *14*, 639–647.

PR9000527

Importance of Neonatal FcR in Regulating the Serum Half-Life of Therapeutic Proteins Containing the Fc Domain of Human IgG1: A Comparative Study of the Affinity of Monoclonal Antibodies and Fc-Fusion Proteins to Human Neonatal FcR

Takuo Suzuki,* Akiko Ishii-Watabe,* Minoru Tada,* Tetsu Kobayashi,* Toshie Kanayasu-Toyoda,* Toru Kawanishi,† and Teruhide Yamaguchi*

The neonatal FcR (FcRn) binds to the Fc domain of IgG at acidic pH in the endosome and protects IgG from degradation, thereby contributing to the long serum half-life of IgG. To date, more than 20 mAb products and 5 Fc-fusion protein products have received marketing authorization approval in the United States, the European Union, or Japan. Many of these therapeutic proteins have the Fc domain of human IgG1; however, the serum half-lives differ in each protein. To elucidate the role of FcRn in the pharmacokinetics of Fc domain-containing therapeutic proteins, we evaluated the affinity of the clinically used human, humanized, chimeric, or mouse mAbs and Fc-fusion proteins to recombinant human FcRn by surface plasmon resonance analysis. The affinities of these therapeutic proteins to FcRn were found to be closely correlated with the serum half-lives reported from clinical studies, suggesting the important role of FcRn in regulating their serum half-lives. The relatively short serum half-life of Fc-fusion proteins was thought to arise from the low affinity to FcRn. The existence of some mAbs having high affinity to FcRn and a short serum half-life, however, suggested the involvement of other critical factor(s) in determining the serum half-life of such Abs. We further investigated the reason for the relatively low affinity of Fc-fusion proteins to FcRn and suggested the possibility that the receptor domain of Fc-fusion protein influences the structural environment of the FcRn binding region but not of the FcγRI binding region of the Fc domain. *The Journal of Immunology*, **2010, 184: 1968–1976.**

In healthy humans, IgG1 exhibits a long serum half-life of ~21 d (1). This prolonged half-life of IgG can be explained by the interaction with neonatal FcR (FcRn). FcRn is a heterodimer of the MHC class I-like H chain and the β_2-microglobulin (β_2m) L chain (2). Although this receptor was originally studied as a transporter of IgG from mother to fetus, subsequent studies have shown that this receptor also plays a critical role in regulating IgG homeostasis (3, 4). FcRn binds to the Fc domain of IgG at pH 6.0–6.5 but not, or weakly, at pH 7.0–7.5 (5). Therefore, FcRn protects IgG from degradation by binding to IgG in endosome and releases IgG into plasma (6). As indicated by previous studies in which amino acid substitutions in the Fc domain of IgG for modifying the affinity to FcRn can alter the serum half-life of the IgG, the affinity to FcRn is thought to play a critical role in determining the serum half-life of IgG (7–12).

Recently, therapeutic use of mAb products has become more important for various diseases, including cancer as well as autoimmune and infectious diseases (6, 13, 14). In addition to the mAbs, the Fc-fusion proteins (e.g., etanercept, alefacept, and abatacept) have been developed and have received considerable attention. These Fc-fusion proteins consist of an extracellular domain of membrane receptor linked to the Fc portion of human IgG1. They work like Abs by binding to ligands for the receptors. The receptor portions of etanercept and alefacept are, respectively, the extracellular ligand-binding portion of the human 75-kDa TNFR and the extracellular CD2-binding portion of the human leukocyte function Ag 3. Abatacept consists of the extracellular domain of human CTLA-4 linked to the modified Fc portion of human IgG1.

Most of the mAb products and Fc-fusion protein products have the Fc domain of human IgG1 (6, 14). Accumulating evidence regarding their clinical use has revealed that their serum half-lives are variable, ranging from 4 to 23 d, regardless of the presence of the Fc domain of human IgG1 (6). Although many factors such as m.w., posttranslational modifications including glycosylation, electrical properties, interactions with FcRs or target molecules, and features of the target molecules may influence their serum half-life, the reasons for the variability of half-life have not been elucidated. Among such factors, FcRn might play a critical role in regulating half-life; however, comparative studies between the affinities of these therapeutic proteins to FcRn and their half-lives in humans have not been reported. Therefore, although some Fc domain-containing therapeutic proteins exhibit shorter half-lives in humans, it remains unclear whether the shorter half-lives are due to the lower affinity to FcRn or other factors.

*Division of Biological Chemistry and Biologicals and †Division of Drugs, National Institute of Health Sciences, Tokyo, Japan

Received for publication October 8, 2009. Accepted for publication December 16, 2009.

This work was supported in part by Grant-in-Aid for Young Scientists 21790172 from the Ministry of Education, Culture, Sports, Science, and Technology, and Grants-in-Aid for Scientific Research 18590163 and 20590167 from Japan Society for the Promotion of Science.

Address correspondence and reprint requests to Dr. Akiko Ishii-Watabe, National Institute of Health Sciences, 1-18-1 Kamiyoga, Setagaya-ku, Tokyo 158-8501, Japan. E-mail address: watabe@nihs.go.jp

Abbreviations used in this paper: β_2m, β_2-microglobulin; FcRn, neonatal FcR; HER2, human epidermal growth factor receptor 2; ND, not detected; R^2, coefficient of determination; SPR, surface plasmon resonance.

www.jimmunol.org/cgi/doi/10.4049/jimmunol.0903296

In this study, we examined the affinity of clinically used mAbs and Fc-fusion proteins to recombinant human FcRn by surface plasmon resonance (SPR) analysis. The analytes used were human Ab (adalimumab), humanized Abs (daclizumab, omalizumab, palivizumab, and trastuzumab), chimeric Abs (infliximab and rituximab), mouse Ab (muromonab-CD3), and Fc-fusion proteins (etanercept, alefacept, and abatacept). We found that the affinities of the therapeutic proteins tested to FcRn were closely correlated with their serum half-lives, with a few exceptions. Because Fc-fusion proteins, which have relatively short half-lives (4–13 d), were shown to have lower affinity to FcRn than mAbs, we further investigated the reason for this difference by examining the affinity of the proteins to FcγRI or the affinity of papain-digested proteins to FcRn in SPR analyses. Our results suggested the possibility that the receptor portions of Fc-fusion proteins make a difference in the higher-order structure of the FcRn-binding region of Fc (i.e., CH2-CH3 interface) or interfere with binding between the Fc domain and FcRn by steric hindrance.

Materials and Methods

Therapeutic proteins and reagents

Abatacept (Bristol-Myers Squibb, Princeton, NJ), adalimumab (Abbott, Baar, Switzerland), alefacept (Biogen Idec, Cambridge, MA), daclizumab (Hoffmann-La Roshe, Nutley, NJ), etanercept (Takeda Pharmaceutical, Osaka, Japan), infliximab (Tanabe Pharmaceutical, Osaka, Japan), muromonab-CD-3 (Jansen Pharmaceutical, Tokyo, Japan), omalizumab (Novartis Pharma Schweiz, Bern, Switzerland), palivizumab (Abbott Japan, Osaka, Japan), rituximab (Zenyaku Kogyo, Tokyo, Japan), and trastuzumab (Chugai Pharmaceutical, Tokyo, Japan) were purchased via reagent distributors. Recombinant human TNF-α was purchased from Wako (Osaka, Japan).

Purification of human FcRn

Stably transfected CHO cells expressing both the soluble portion of the hFcRn H chain (residues 1–267 of mature protein) and β_2m were provided by P. J. Bjorkman (California Institute of Technology, Pasadena, CA). Expression and purification of hFcRn were performed according to the method previously reported by West and Bjorkman (15), with slight modifications. Briefly, the CHO cells expressing soluble hFcRn and β_2m were cultured in α-MEM containing 5% dialyzed FBS, 100 μM methionine sulfoximine, and penicillin/streptomycin. Cell culture supernatant was collected every 2–3 d and was filtered with a 0.45-μm filter, and sodium azide was then added to 0.05%. The harvested supernatant was acidified to pH 5.8 and then applied to a human IgG column. After washing the column with 50 mM Bis-Tris (pH 5.8), hFcRn complexed with β_2m was eluted with 40 mM Bis-Tris/20 mM Tris (pH 8.1). The eluted fractions containing hFcRn were applied to a Uno-Q1 column, and hFcRn was eluted with pH gradient using 40 mM Bis-Tris/20 mM Tris (pH 8.1) and 40 mM Bis-Tris/20 mM Tris (pH 5.8).

SDS-PAGE and Western blotting

Each fraction of protein eluted from the Uno-Q1column was diluted in 1× SDS loading buffer and was separated in 15% polyacrylamide gel (Bio craft, Tokyo, Japan). After the electrophoresis, the gels were stained with Imperial protein stain (Pierce, Rockford, IL). For Western blotting, proteins separated by SDS-PAGE were electroblotted onto polyvinylidene difluoride membranes (Millipore, Billerica, MA). The membranes were immunoreacted with rabbit anti-hFcRn H chain peptide (Leu^{135}-Gly^{148}) Ab produced by Medical and Biological Laboratories (Nagoya, Japan) and then with HRP-conjugated secondary Abs (Cell Signaling Technology, Danvers, MA). The bands of hFcRn were detected using ECL Plus Western blotting detection reagents (Amersham Biosciences, Piscataway, NJ).

SPR analyses

Analysis of affinity between FcRn and Fc domain-containing therapeutic proteins. The purified recombinant hFcRn was diluted with 10 mM sodium acetate (pH 5.0 or 4.5) and was immobilized onto a CM5 biosensor chip (Biacore, Uppsala, Sweden) using an amine coupling kit (Biacore) at relatively low densities (mainly 300–350 resonance units) to avoid mass transport limitation. The reference cell was treated with *N*-hydroxysuccinimide/1-ethyl-3-(3-dimethylaminopropyl) carbodiimide and ethanol amine using an amine coupling kit without injecting the FcRn. Fc domain-containing proteins were diluted with the running buffer (50 mM sodium phosphate/150 mM NaCl [pH 6.0]) and injected at 25°C. The running buffer was allowed to flow at a rate of 20 μl/min. The injections were performed using the KINJECT mode (volume, 40 μl; dissociation time, 150 s). For regeneration, the regeneration buffer (100 mM Tris/200 mM NaCl [pH 8.0]) was injected for 4 min. Kinetic constants were calculated from the sensorgrams using the bivalent analyte model of BIAevaluation software 4.1.

To obtain the consistent results, we would indicate two points. First, it is necessary to set the bulk refractive index to zero to avoid wrong fitting, because the binding is rapidly reached to the near-equilibrium state. Second, it is necessary to set the injection point correctly. For example, if the sensorgrams of infliximab shown in Fig. 2 were analyzed with the injection point shifted to 0.5 s earlier, the values of k_{a1}, k_{d1}, and K_D were 1.95E+05 $M^{-1}s^{-1}$, 0.136 s^{-1}, and 697 nM, respectively. When the injection points of the sensorgrams are unclear, it may be better to use the average values of data resulting from two or more different injection points.

Analysis of affinity between FcγRI and Fc domain-containing therapeutic proteins. Recombinant human FcγRI, which consists of human FcγRI (Gln^{16}-Pro^{288}) and His-tag, was purchased from R&D Systems (Minneapolis, MN). Fc domain-containing proteins were immobilized to a CM5 biosensor chip in 10 mM sodium acetate (pH 5.0) using an amine coupling kit. Kinetic analyses of FcγRI binding were performed according to Ellsworth et al. (16) with some modifications. The running buffer, HBS-EP (10 mM HEPES, 150 mM NaCl, 3 mM EDTA, and 0.005% Surfactant P20 [pH 7.4]) (Biacore), was allowed to flow at 20 μl/min. The injections of FcγRI were performed using the KINJECT mode (volume, 40 μl; dissociation time, 150 s). To regenerate the immobilized proteins, the regeneration buffer (10 mM glycine-HCl [pH 1.8]) was injected for 15 s. Kinetic constants were derived from the sensorgrams using the 1:1 binding model of BIAevaluation software 4.1.

Papain digestion

The papain (Wako) was activated in the buffer (50 mM sodium phosphate/150 mM NaCl [pH 6.0], 1 mM cysteine, 4 mM EDTA, and 1 mg/ml papain) at 37°C for 15 min. Next, 1 mg/ml Ab or Fc-fusion protein was digested with 0.1 mg/ml activated papain in 50 mM sodium phosphate (pH 6.0), 150 mM NaCl, 0.1 mM cysteine, and 4 mM EDTA at 37°C for 24 h.

Results

Purification of soluble human FcRn

FcRn binds to the Fc domain at acidic pH and then releases it at neutral pH. Recombinant soluble hFcRn expressed from CHO cells was purified using a human IgG column by binding at pH 5.8 and releasing at pH 8.1. The fraction purified by the IgG column was electrophoresed at lane 10 of SDS-PAGE gel (Fig. 1*B*). This fraction was then purified using an anion-exchange column with a pH gradient elution. The elution diagram is shown in Fig. 1*A*. Three main peaks were observed. The proteins in these peaks were electrophoresed (Fig. 1*B*) and subjected to Western blot analysis using anti-hFcRn H chain peptide Ab (Fig. 1*C*). Several bands were observed at ~32 kDa in these fractions, and these bands were immunoreactive to anti-hFcRn H chain peptide Ab. These results indicated that the purified FcRn had several isoforms, possibly because of the difference in posttranslational modification, including glycosylation or proteolysis. As shown in Fig. 1*C*, the signals of the higher m.w. bands of hFcRn tend to be weak. There is a possibility that the sugar chain at Asn^{125} of hFcRn interfered with the reactivity of the hFcRn to the anti-hFcRn H chain peptide Ab used. We analyzed the affinity of therapeutic mAbs and Fc fusion proteins to FcRn by SPR using the peak I, II, or III fractions eluted from the anion-exchange column. The K_D values were higher when peak I was used as a ligand in SPR analyses than when peaks II or III were used (data not shown). Because the m.w. of the proteins in peak I was smaller than that in peak II/III and the protein content of peak I varied depending on the lot of the cell culture supernatant, peak I seemed to consist of immature FcRn. The K_D values calculated from the experimental data using peaks II and III were comparable (data not shown). We, therefore, used the main peak (i.e., peak III) in the following experiments.

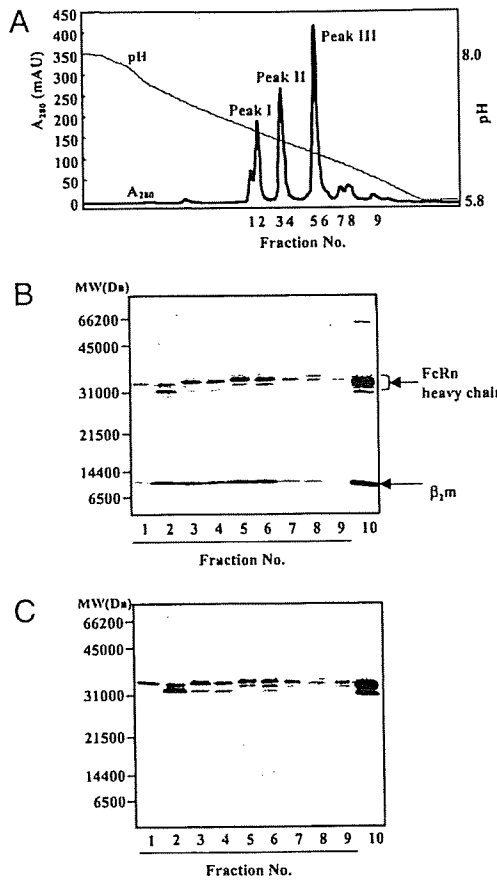

FIGURE 1. Purification and electrophoretic characterization of recombinant human FcRn. *A*, The elution diagram of the anion-exchange chromatography used for the purification of recombinant human FcRn. *B*, SDS-PAGE of the proteins in the fractions indicated in *A*. The protein applied to the anion-exchange column was electrophoresed in *lane 10*. The gel was stained with Imperial protein stain. *C*, Western blot analysis of eluate from the anion-exchange column by anti-hFcRn H chain Ab.

SPR analyses of the affinity between FcRn and Fc domain-containing proteins

Purified FcRn was immobilized onto a CM5 biosensor chip at relatively low densities as described in *Materials and Methods*. Five or six concentrations of Fc domain-containing therapeutic proteins were then injected. Because injection at higher concentrations caused nonspecific binding to flow cells, we analyzed the affinity of therapeutic proteins using sensorgrams obtained at the concentrations at which nonspecific binding was not observed. For example, infliximab was injected at concentrations of 670, 335, 168, 84, and 42 nM, and we analyzed the affinity to FcRn with the bivalent analyte model (Fig. 2). The colored lines were observed sensorgrams, and the black lines were fitting lines generated by the BIAevaluation software. The K_D value ($= k_{d1}/k_{a1}$) calculated from these sensorgrams was 727 nM. The affinities of adalimumab and etanercept to FcRn were 672 and 3612 nM, respectively (Fig. 2).

The affinities of the 11 kinds of Fc domain-containing proteins to FcRn were measured (Fig. 3). Adalimumab, daclizumab, infliximab, palivizumab, and rituximab were injected at concentrations of 42–670 nM. The concentrations of abatacept, alefacept, and etanercept used were 168–5360 nM, and those of muromonab-CD3, omalizumab, and trastuzumab were 84–1340 nM. Under this condition, the tested therapeutic proteins, except for muromonab-CD3, bound to FcRn. The K_D values measured in our experiments and the serum half-lives in humans reported in the literature are shown in Fig. 3*A*.

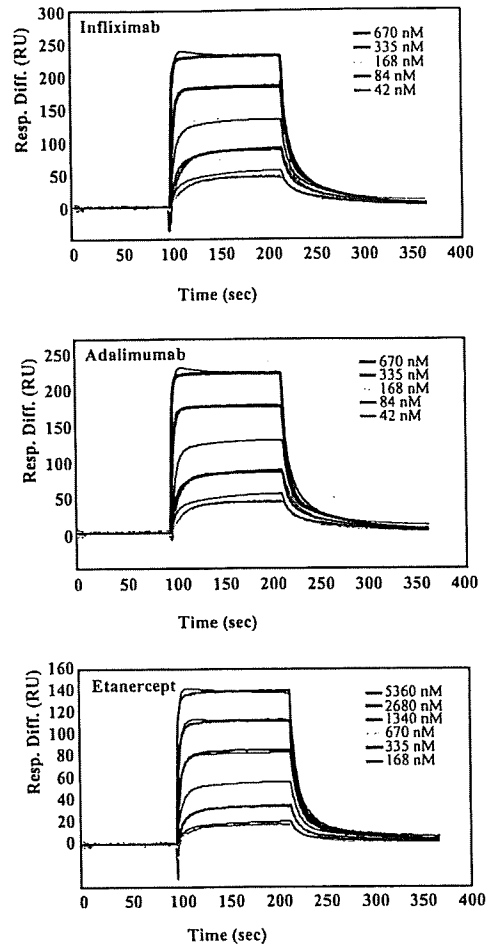

	Infliximab	Adalimumab	Etanercept
k_a1 (1/Ms)	2.09E+05	2.41E+05	3.71E+04
k_d1 (1/s)	0.152	0.162	0.134
k_a2 (1/RUs)	4.56E-05	3.98E-05	3.27E-05
k_d2 (1/s)	9.78E-03	8.80E-03	5.44E-03
Rmax (RU)	3.76E+02	3.47E+02	1.93E+02
Chi2	1.80E+01	1.74E+01	5.37E+00
$K_D=k_d1/k_a1$	727 nM	672 nM	3612 nM

FIGURE 2. Representative sensorgrams of SPR analyses. Infliximab (*upper panel*) or adalimumab (*middle panel*) was injected at concentrations of 42–670 nM and etanercept (*lower panel*) at concentrations of 168–5360 nM. The colored lines are the observed sensorgrams, and the black lines are fitting lines generated by the bivalent analyte model of BIAevaluation software. The association of KINJECT was started at ~100 s, and the dissociation of KINJECT was at ~220 s. The table describes the kinetic values calculated from the sensorgrams of infliximab, adalimumab, and etanercept.

The K_D values and the average values of the serum half-lives are plotted in Fig. 3*B*. The K_D values were closely correlated to the half-lives (contribution ratio = 0.8675) when the results were analyzed after excluding the data for infliximab, rituximab, and trastuzumab (Fig. 3*C*). Concerning infliximab, rituximab, and trastuzumab, which have relatively short half-lives and comparable affinity to other long half-life Abs to FcRn, other critical factor(s) seemed to be involved in regulating their half-lives (see *Discussion*). Although it was impossible to plot the data for mouse mAb muromonab-CD3,

A

Structure	Nonproprietary name	Binding target	Affinity to FcRn K_D (nM)	Half-life (days)	cited from the literature
Human antibody	Adalimumab	TNFα	672	14.7-19.3	Weisman et al., 2003
Humanized antibody	Daclizumab	CD25	846	20	Vincenti et al., 1998
	Omalizumab	IgE	1237	20	Casale et al., 1997
	Palivizumab	RSV F protein	750	19-27	Subramanian et al., 1998
	Trastuzumab	HER2	773	2.7-10	Tokuda et al., 1999
Chimeric antibody	Infliximab	TNFα	727	9.5	Comillie et al., 2001
	Rituximab	CD20	508	9.4	Maloney et al., 1997
Mouse antibody	Muromonab-CD3	CD3	ND	0.75	Hooks et al., 1991
Fc-fusion protein	Abatacept	CD80/CD86	2633	13.1	prescribing information
	Alefacept	CD2	2506	11.3	prescribing information
	Etanercept	TNFα	3612	4	Lee et al., 2003

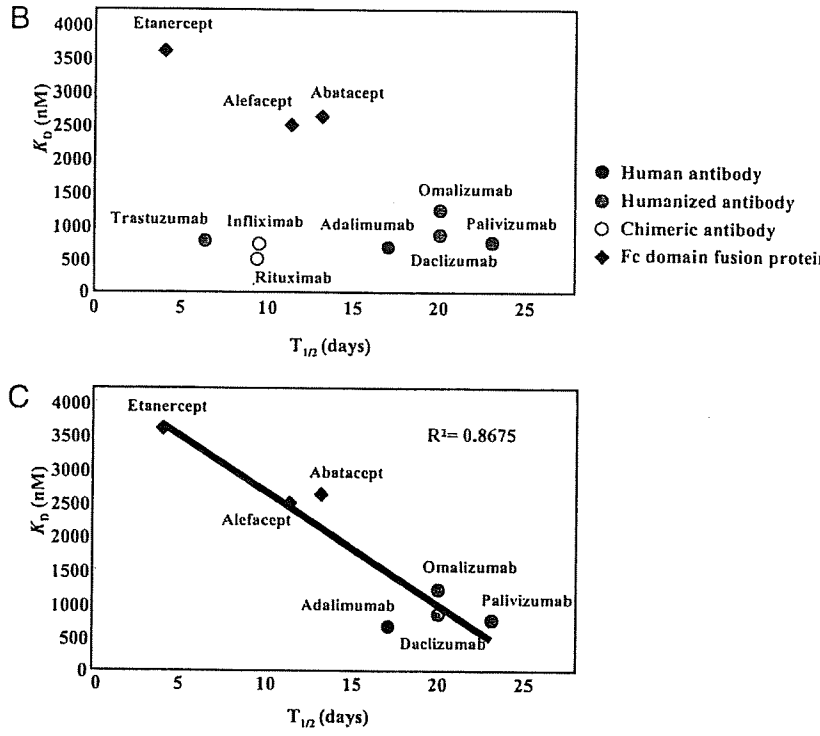

FIGURE 3. K_D values of binding between Fc domain-containing therapeutic proteins and hFcRn and the correlation with their serum half-lives. *A*, The K_D values obtained in our study and the half-lives in humans cited from the literature. The half-life values were obtained from the article reviewed by Lobo et al. (6) [adalimumab (17), daclizumab (18), etanercept (19), infliximab (20), muromonab-CD3 (21), omalizumab (22), palivizumab (23), rituximab (24), and trastuzumab (25)] or from the manufacturer prescribing information. *B*, The graphical presentation of the K_D values and serum half-lives described in *A*. The means of half-lives are plotted on the *x*-axis, and the values of affinity to FcRn are on the *y*-axis. Filled rhombi, Fc domain fusion proteins; closed circle, human Ab; gray circles, humanized Abs; open circle, chimeric Abs. *C*, Regression line of the plots of seven therapeutic proteins. ND, not detected; R^2, coefficient of determination.

which exhibited no significant binding to human FcRn, the half-life of this Ab in humans is the shortest (0.75 d) among the therapeutic proteins examined in this study (21). These results also show the importance of the binding affinity to FcRn in determining the serum half-life. The correlation described above was also observed when other fractions of hFcRn described in Fig. 1 (peaks I and II) were used in SPR analyses (data not shown).

The affinity between FcγRI and Fc domain-containing proteins

Because the affinities of Fc fusion proteins (etanercept, alefacept, and abatacept) to FcRn were lower than those of mAbs, the FcRn-binding region (CH2-CH3 domain interface) of Fc-fusion proteins seems to be structurally different from that of mAbs. We also analyzed the affinity of these proteins to FcγRI to test whether the structural environment around the FcγRI-binding region (hinge proximal region of CH2) is different between Fc-fusion proteins and Abs. Because the regeneration procedure in the SPR assay inactivated FcγRI but not Fc domain-containing therapeutic proteins, therapeutic proteins were immobilized to CM5 biosensor chips, and FcγRI was used as an analyte. The sensorgrams of Fc-fusion proteins (abatacept, alefacept, and etanercept) and mAbs (adalimumab and infliximab) are shown in Fig. 4*A*. The data were analyzed with a 1:1 binding model. The K_D values of the two Fc fusion proteins (alefacept and etanercept) and Abs (adalimumab and infliximab) were comparable (Fig. 4*B*). The K_D values obtained in this study were similar to the data reported for IgG [reviewed by van de Winkel and Anderson (26)]. In contrast, abatacept had a lower affinity to FcγRI. In abatacept, a series of selected mutations those can alter the binding affinity to FcγR were introduced to reduce Fc-mediated cytotoxic effects (Fig. 5) (28, 29). Therefore, the data in Fig. 4 show that the change in the affinity of Fc domain to FcγRI, which is caused by amino acid substitutions, was detected in our experiments. These results suggest that the region interacting with FcγRI (i.e., the hinge proximal region of CH2) was not structurally different between Fc fusion proteins, except for abatacept, and Abs examined.

The affinity between FcRn and Fc domains generated by papain treatment

In Fig. 5, the amino acids sequences of abatacept, alefacept, etanercept, adalimumab, infliximab, and omalizuamb are aligned. The differences in the primary structure of the Fc regions were Glu^{376} and Met^{378} of etanercept, which are attributed to the IgG1 allotype, and Ser^{162}, Ser^{165}, and Ser^{174} of abatacept, which are due

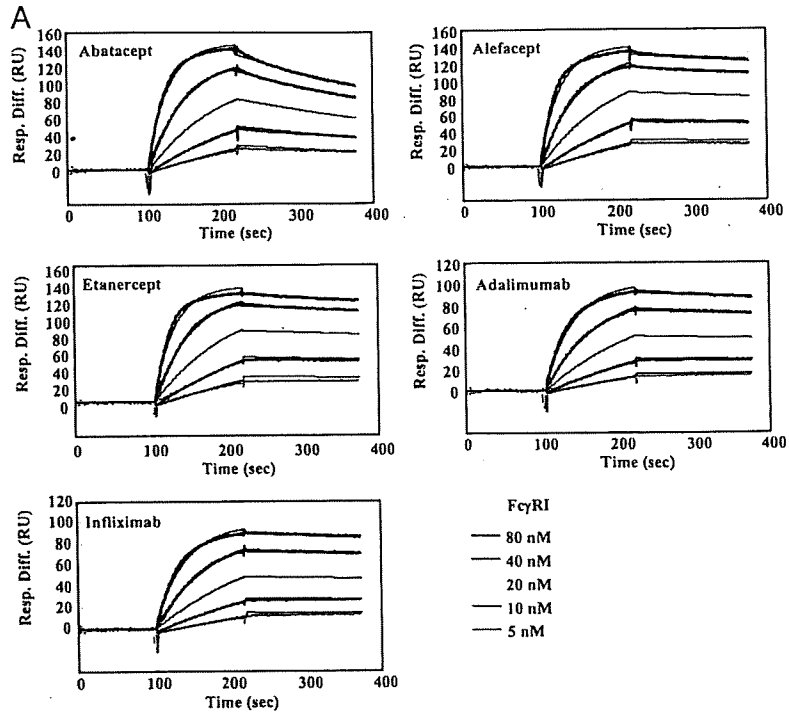

B

	Affinity to FcγRI K_D (nM)
Abatacept	4.82
Alefacept	0.857
Etanercept	0.818
Adalimumab	0.779
Infliximab	0.763

FIGURE 4. The affinity of Fc-fusion proteins and Abs to FcγRI. The Fc-fusion proteins (abatacept, alefacept, and etanercept) and mAbs (adalimumab and infliximab) were immobilized onto CM5 biosensor chips. Recombinant protein of the extracellular domain of FcγRI was injected at concentrations of 5–80 nM and analyzed with a 1:1 binding model (*A*). The colored lines are the observed sensorgrams, and the black lines are fitting lines. Association phase, ~100–220 s; dissociation phase, ~220 s. *B*, The K_D values calculated from the sensorgrams shown in *A*.

to the engineering for decreasing affinity to FcγR and improving protein production (28). To test the possibility that this limited structural difference or posttranscriptional modifications such as glycosylation can give rise to the difference in binding affinity to FcRn, we digested the Fc-fusion proteins or mAbs with papain and analyzed the affinity of their Fc domains to FcRn. The electrophoretic pattern of etanercept and adalimumab digested with papain is shown in Fig. 6*A*. Both etanercept and adalimumab were digested sufficiently for 24 h at 37°C under the conditions described in *Materials and Methods*, whereas digestion was not sufficient after incubating for 2 h. Therefore, the therapeutic proteins digested with papain for 24 h were used for the SPR analyses. The sensorgrams of etanercept (670 nM) and adalimumab (670 nM) were much different without incubation with papain, but they became almost identical after papain digestion (Fig. 6*B*). We measured the affinities to FcRn of five therapeutic proteins (etanercept, alefacept, adalimumab, infliximab, and omalizumab) digested with papain (Fig. 6*C*). Etanercept and alefacept are Fc-fusion proteins with low affinity to FcRn, and omalizumab is an Ab showing lower affinity to FcRn than other Abs. Because it was possible that the proteins were cleaved, in part, into smaller fragments than the Fc domain, the estimated K_D values may have been larger than the actual values. However, it was very clear that the affinities of etanercept, alefacept, infliximab, and omalizumab were increased by papain treatment (Fig. 6*C*).

The affinity of Fc-fusion protein and Abs became comparable after papain digestion, showing that the differences in amino acid sequences or posttranslational modification of the Fc domain did not contribute to the difference in the binding affinity of these proteins to FcRn. It therefore seems likely that the receptor domain of the Fc-fusion protein makes a difference in the higher-order structure of the FcRn-binding region of Fc (i.e., CH2-CH3 interface) or interferes with the binding between Fc domain and FcRn by steric hindrance. Moreover, such a difference or interference seems to be involved in determining the affinity to FcRn for some kinds of Abs, because the K_D values of infliximab and omalizumab were also increased significantly by papain treatment.

The affinity between FcRn and therapeutic proteins binding with target molecules

On the basis of the results suggesting the possibility that another region besides the Fc domain influences the affinity of Fc domain-containing proteins to FcRn, we assumed that binding with the target molecule would also change the affinity to FcRn. Because adalimumab, infliximab, and etanercept bind to the same target molecule, TNF-α, we analyzed the effects of binding with TNF-α on the affinity of these therapeutic proteins to FcRn. First, 0–2680 nM TNF-α was added to 335 nM infliximab and incubated for at least 1 h. The resulting mixture was then injected into the flow cell, and the affinities to FcRn were analyzed. By adding TNF-α, the shape of the sensorgram was drastically altered (Fig. 7*A*). The Abs (adalimumab and infliximab) can maximally bind to two TNF-α trimers, whereas etanercept binds to one TNF-α trimer. When the relative concentrations of TNF-α are low, three molecules of the Ab can bind to each TNF-α trimer, and cross-linked TNF/Ab complexes are formed (30). To evaluate the affinity

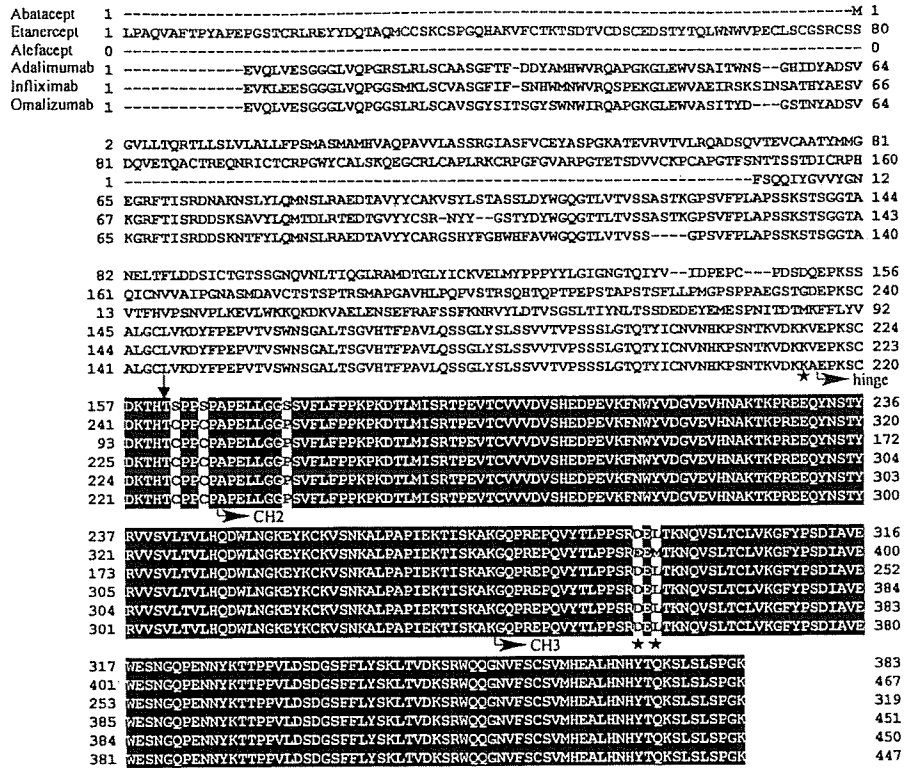

FIGURE 5. The amino acid sequences of abatacept, alefacept, etanercept, and H chains of adalimumab and infliximab. The amino acids marked with a star are different among allotypes of IgG1. The gray arrow is the cleavage site of IgG1 with papain (27). The amino acid sequences were obtained from the following links: abatacept, http://whqlibdoc.who.int/druginfo/18_2_2004_INN91.pdf; alefacept, http://whqlibdoc.who.int/druginfo/DRUG_INFO_14_4_2000_INN-84.pdf; etanercept, http://whqlibdoc.who.int/druginfo/DRUG_INFO_13_2_1999_INN-81.pdf; adalimumab, www.info.pmda.go.jp/shinyaku/g080405/10015900_22000AMX01598_A100_1.pdf; infliximab, www.info.pmda.go.jp/shinyaku/g020102/40031500_21400AMY00013_Q100_2.pdf; and omalizumab, www.drugbank.ca/drugs/DB00043.

between FcRn and TNF-α–binding proteins, excess TNF-α was added to adalimumab, infliximab, and etanercept (8-fold molar excess to 42–670 nM Abs and 4-fold to 168–2680 nM etanercept) to avoid forming nonuniform complexes. The sensorgrams were fitted by the bivalent analyte model (Fig. 7*B*). Although the fitted lines did not completely match the observed sensorgrams, the K_D values of infliximab, adalimumab, and etanercept to FcRn were calculated to be 2057, 1321, and 4286 nM, respectively (Fig. 7*C*). The affinity of infliximab–TNF-α complex or adalimumab–TNF-α complex was lower than that of infliximab or adalimumab, respectively (Fig. 7*C*). These results suggest that at least for these anti–TNF-α Abs, binding with target molecules decreases the affinity to FcRn. They may also suggest that the anti–TNF-α Abs complexed with TNF-α will be degraded more rapidly than anti–TNF-α Abs free from TNF-α in vivo.

Discussion

To our knowledge, this is the first article to elucidate the affinities of clinically used Fc domain-containing therapeutic proteins to FcRn in a comparative study. Because the affinities of these therapeutic proteins to FcRn were found to be highly correlated with the serum half-lives in humans, with the exception of infliximab, rituximab, and trastuzumab, the importance of FcRn in regulating the serum half-life of Fc domain-containing therapeutic proteins was suggested. The key observation was that the Fc-fusion proteins showed lower affinity to FcRn than Abs. These data provided us with one of the answers to the question of why the Fc-fusion proteins containing the Fc domain of human IgG1 exhibit a shorter half-life than human IgG1.

In the current study, we used the bivalent analyte model of BIAevaluation software. Most studies analyzing Fc-FcRn interactions have used the bivalent analyte model (15, 31) or the heterogeneous ligand model (7, 15, 31). Although the sensorgrams in our experiments were able to be fitted by both models, they were better fitted by the bivalent analyte model. Considering that two molecules of hFcRn bind to each IgG, resulting in a 2:1 binding stoichiometry (15), the bivalent analyte model seems to be suitable. It has been reported that the dual bivalent analyte model better fits the data of the FcRn-Fc interaction (32), although there are cases in which the bivalent analyte model does not work well. In the article about the dual bivalent analyte model, it was speculated that high-affinity and low-affinity types of FcRn existed on the surface of the BIAcore chip and that the low-affinity type receptor was probably an experimental artifact (32). Possibly because the content of the low-affinity type of FcRn on the chip is comparatively low in our immobilizing condition, the sensorgrams in our experiments might have been well-fitted by the bivalent analyte model.

Among the therapeutic proteins tested in this study, the Fc fusion proteins showed relatively lower affinities to FcRn (Figs. 2, 3), although the affinities to FcγRI are comparable to those of Abs (Fig. 4). Although the Fc domain binds to FcRn via the CH2-CH3 domain interface (33), the primary structures of the Fc domains of tested therapeutic proteins were almost the same, and cleavage of the Fc domains from Fab or the receptor region gave similar K_D values to FcRn (Fig. 6). These results suggest that the receptor regions of Fc-fusion protein alter the conformation of the FcRn-binding region (CH2-CH3 domain interface), not of the FcγRI-binding region (hinge proximal region of CH2 domain), or cause steric hindrance on the CH2-CH3 domain interface. The influence of regions besides the Fc domain on FcRn-binding regions would also be the case for Abs, as shown in Fig. 7.

Our results presented in this study can provide valuable information regarding the molecular design of novel Fc domain-containing therapeutic proteins and demonstrate the usefulness of FcRn-binding analysis in the characterization of Fc domain-containing therapeutic proteins. In addition to the Fc fusion proteins used in this study, rilonacept, a Fc-fusion protein consisting of ligand-binding domains of the extracellular portions of the human IL-1 receptor component (IL-1RI) and IL-1 receptor accessory protein linked to the Fc portion of human IgG1, and romiplostim,

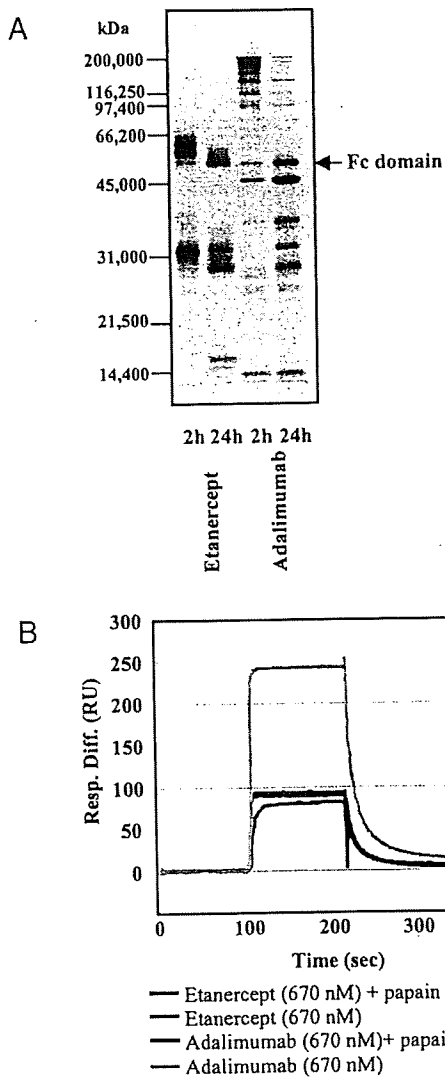

FIGURE 6. Effects of papain digestion on the affinities of Fc domain-containing therapeutic proteins to FcRn. *A*, The nonreduced SDS-PAGE of etanercept and adalimumab digested with papain for 2 and 24 h. *B*, The comparison between the sensorgrams of etanercept and adalimumab with or without papain digestion. *C*, Comparison of the affinity to FcRn among etanercept, alefacept, adalimumab, infliximab, and omalizumab, which were digested or not digested with papain. The K_D values were calculated from the sensorgrams at the range of concentrations described as follows. The concentrations of papain-digested etanercept, papain-digested alefacept, adalimumab, papain-digested adalimumab, infliximab, papain-digested infliximab, and papain-digested omalizumab were 42–670 nM; those of etanercept and alefacept were 168–5360 nM, and those of omalizumab were 42–1340 nM. Each bar shows the average K_D value + SD, which was calculated from three independent experiments. $^{**}p < 0.01$. NS, no significant difference according to Student *t* test.

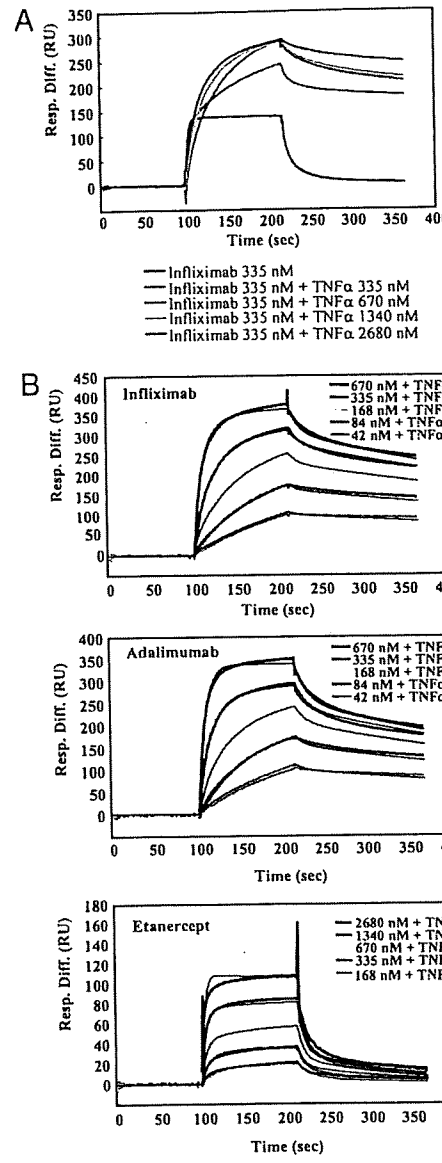

C

	Affinity to FcRn K_D (nM)	
	control	preincubate with TNFα
Etanercept	3705	4286
Adalimumab	673	1321
Infliximab	751	2057

FIGURE 7. Effects of binding with the target molecules on the affinities of Fc domain-containing therapeutic proteins to FcRn. *A*, The sensorgrams of infliximab (335 nM) preincubated with TNF-α (0–2680 nM). *B*, The sensorgrams of infliximab (*upper panel*), adalimumab (*middle panel*), and etanercept (*lower panel*) preincubated with TNF-α (8-fold molar excess to 42–670 nM Abs and 4-fold to 168–2680 nM etanercept). The sensorgrams were fitted by the bivalent analyte model. *C*, The K_D values calculated from the sensorgrams shown in *B*. The values of infliximab, adalimumab, and etanercept derived from the same series of experiments are also shown as controls.

a Fc-peptide fusion protein consisting of human IgG1 Fc domain linked at the C terminus to a peptide containing two thrombopoietin receptor-binding domains, were approved recently (34, 35). The

development of Fc-fusion proteins will receive further attention. Although the Fc domains are used with the intent of prolonging the half-lives of receptor proteins, the half-lives tend not to be fully prolonged to the level of IgG1. It remains unclear whether the receptor regions of Fc-fusion proteins alter the conformation of the CH2-CH3 domain interface or the regions cause steric hindrance on the binding site of FcRn; however, the molecular design of Fc-fusion proteins having a higher affinity to FcRn might be possible in either case.

Reflecting the increasing interest in the development of mAbs and related products, the newly revised guideline for such products was adopted by the European Medicines Agency in 2008 (www.emea.europa.eu/pdfs/human/bwp/15765307enfin.pdf). In the guidelines, it is mentioned that FcRn-binding activity should be provided, as appropriate, in product characterization. Because regions other than the Fc domain might affect the affinity of the protein to FcRn (Figs. 6, 7), the affinity to FcRn should be evaluated as an important quality attribute related to the pharmacokinetic profile, even if the protein has a native Fc domain of IgG1, especially in cases of Fc-fusion proteins. Meanwhile, because it was demonstrated that oxidation of two labile methionines, Met^{252} and Met^{428}, in human IgG1 attenuates binding of the Ab to FcRn (36), alteration of the affinity to FcRn during the production process or storage will reflect structural changes of the protein, including Met oxidation, that will lead to shortening the serum half-life. In addition to IgG, albumin is also known to bind to FcRn in a pH-dependent manner and is protected from degradation (37, 38). The albumin-fusion proteins (e.g., albumin-IFN) or drugs having an albumin-binding moiety are being developed. FcRn-binding characteristics would also be important as a quality attribute of such products, which is related to the pharmacokinetic profile.

As mentioned above, the existence of several Abs having a short half-life and high affinity to FcRn suggested the involvement of other critical factor(s) in regulating the serum half-life of Abs such as trastuzumab, rituximab, or infliximab. Trastuzumab is a humanized Ab directed against human epidermal growth factor receptor 2 (HER2), which is expressed in some types of breast cancer cells. It has been reported that trastuzumab is taken up by HER2-expressing cells via HER2-mediated endocytosis (39, 40). Rituximab, a chimeric Ab directed against CD20, is also internalized in an Ag-mediated manner (41). Because the ligand-dependent internalization is followed by degradation of Abs, this property seems to be an important reason for the short half-life of trastuzumab and rituximab. It has been reported that, in general, the half-life of monoclonal IgG Abs increases depending on the degree of humanization in the order of murine < chimeric < humanized < human (6, 41, 42). Because infliximab and rituximab are chimeric Abs, the involvement of common factors influencing the half-life of chimeric Abs such as the presence of human anti-chimeric Ab would be another reason for the shorter half-life.

As shown in Fig. 7, the affinities of infliximab–TNF-α complex and adalimumab–TNF-α complex seemed to be lower than those of infliximab and adalimumab. If the affinity of therapeutic proteins/target molecules complexes to FcRn is lower than that of the free therapeutic proteins, the complexes will be degraded faster. Therefore, the half-lives of such therapeutic proteins seem to be shortened in the case that the target molecules are abundant in the bodies of patients. In contrast, if the affinity to FcRn of therapeutic proteins/target molecule complexes is higher than that of the free drugs, the complexes of drug and target molecules will have longer half-lives than free drugs. Because there are many factors affecting the elimination of Abs [reviewed by Tabrizi et al. (41)], further studies are necessary to elucidate the critical factors impacting the half-lives of Fc domain-containing proteins, in addition to the affinity to FcRn. Binding characteristics of the Fc domain-containing proteins or their complex with target molecules to FcγRs would be one of the important issues to be examined in regard to the impact on their elimination.

In conclusion, we showed the importance of the affinity to FcRn in determining the serum half-life of Fc domain-containing therapeutic proteins. Further investigation regarding the molecular structures that regulate the affinity of the engineered protein to FcRn will accelerate the development of therapeutic proteins with a desired half-life.

Acknowledgments

We thank Dr. Pamela Bjorkman for the gift of the cell line expressing FcRn.

Disclosures

The authors have no financial conflicts of interest.

References

1. Morell, A., W. D. Terry, and T. A. Waldmann. 1970. Metabolic properties of IgG subclasses in man. *J. Clin. Invest.* 49: 673–680.
2. Simister, N. E., and K. E. Mostov. 1989. An Fc receptor structurally related to MHC class I antigens. *Nature* 337: 184–187.
3. Junghans, R. P., and C. L. Anderson. 1996. The protection receptor for IgG catabolism is the β_2-microglobulin-containing neonatal intestinal transport receptor. *Proc. Natl. Acad. Sci. USA* 93: 5512–5516.
4. Ghetie, V., S. Popov, J. Borvak, C. Radu, D. Matesoi, C. Medesan, R. J. Ober, and E. S. Ward. 1997. Increasing the serum persistence of an IgG fragment by random mutagenesis. *Nat. Biotechnol.* 15: 637–640.
5. Raghavan, M., V. R. Bonagura, S. L. Morrison, and P. J. Bjorkman. 1995. Analysis of the pH dependence of the neonatal Fc receptor/immunoglobulin G interaction using antibody and receptor variants. *Biochemistry* 34: 14649–14657.
6. Lobo, E. D., R. J. Hansen, and J. P. Balthasar. 2004. Antibody pharmacokinetics and pharmacodynamics. *J. Pharm. Sci.* 93: 2645–2668.
7. Datta-Mannan, A., D. R. Witcher, Y. Tang, J. Watkins, and V. J. Wroblewski. 2007. Monoclonal antibody clearance: impact of modulating the interaction of IgG with the neonatal Fc receptor. *J. Biol. Chem.* 282: 1709–1717.
8. Vaccaro, C., J. Zhou, R. J. Ober, and E. S. Ward. 2005. Engineering the Fc region of immunoglobulin G to modulate in vivo antibody levels. *Nat. Biotechnol.* 23: 1283–1288.
9. Hinton, P. R., J. M. Xiong, M. G. Johlfs, M. T. Tang, S. Keller, and N. Tsurushita. 2006. An engineered human IgG1 antibody with longer serum half-life. *J. Immunol.* 176: 346–356.
10. Dall'Acqua, W. F., P. A. Kiener, and H. Wu. 2006. Properties of human IgG1s engineered for enhanced binding to the neonatal Fc receptor (FcRn). *J. Biol. Chem.* 281: 23514–23524.
11. Petkova, S. B., S. Akilesh, T. J. Sproule, G. J. Christianson, H. Al Khabbaz, A. C. Brown, L. G. Presta, Y. G. Meng, and D. C. Roopenian. 2006. Enhanced half-life of genetically engineered human IgG1 antibodies in a humanized FcRn mouse model: potential application in humorally mediated autoimmune disease. *Int. Immunol.* 18: 1759–1769.
12. Yeung, Y. A., M. K. Leabman, J. S. Marvin, J. Qiu, C. W. Adams, S. Lien, M. A. Starovasnik, and H. B. Lowman. 2009. Engineering human IgG1 affinity to human neonatal Fc receptor: impact of affinity improvement on pharmacokinetics in primates. *J. Immunol.* 182: 7663–7671.
13. Nissim, A., and Y. Chernajovsky. 2008. Historical development of monoclonal antibody therapeutics. In *Therapeutic Antibodies (Handbook of Experimental Pharmacology)*, Vol. 181. Y. Chernajovsky and A. Nissim eds. Springer, New York, p. 3–18.
14. Reichert, J. M., C. J. Rosensweig, L. B. Faden, and M. C. Dewitz. 2005. Monoclonal antibody successes in the clinic. *Nat. Biotechnol.* 23: 1073–1078.
15. West, A. P., Jr., and P. J. Bjorkman. 2000. Crystal structure and immunoglobulin G binding properties of the human major histocompatibility complex-related Fc receptor. *Biochemistry* 39: 9698–9708.
16. Ellsworth, J. L., M. Maurer, B. Harder, N. Hamacher, M. Lantry, K. B. Lewis, S. Rene, K. Byrnes-Blake, S. Underwood, K. S. Waggie, et al. 2008. Targeting immune complex-mediated hypersensitivity with recombinant soluble human FcγRIA (CD64A). *J. Immunol.* 180: 580–589.
17. Weisman, M. H., L. W. Moreland, D. E. Furst, M. E. Weinblatt, E. C. Keystone, H. E. Paulus, L. S. Teoh, R. B. Velagapudi, P. A. Noertersheuser, G. R. Granneman, et al. 2003. Efficacy, pharmacokinetic, and safety assessment of adalimumab, a fully human anti-tumor necrosis factor-α monoclonal antibody, in adults with rheumatoid arthritis receiving concomitant methotrexate: a pilot study. *Clin. Ther.* 25: 1700–1721.
18. Vincenti, F., R. Kirkman, S. Light, G. Bumgardner, M. Pescovitz, P. Halloran, J. Neylan, A. Wilkinson, H. Ekberg, R. Gaston, et al. 1998. Interleukin-2-receptor blockade with daclizumab to prevent acute rejection in renal transplantation. *N. Engl. J. Med.* 338: 161–165.
19. Lee, H., H. C. Kimko, M. Rogge, D. Wang, I. Nestorov, and C. C. Peck. 2003. Population pharmacokinetic and pharmacodynamic modeling of etanercept using logistic regression analysis. *Clin. Pharmacol. Ther.* 73: 348–365.

20. Cornillie, F., D. Shealy, G. D'Haens, K. Geboes, G. Van Assche, J. Ceuppens, C. Wagner, T. Schaible, S. E. Plevy, S. R. Targan, and P. Rutgeerts. 2001. Infliximab induces potent anti-inflammatory and local immunomodulatory activity but no systemic immune suppression in patients with Crohn's disease. *Aliment. Pharmacol. Ther.* 15: 463–473.
21. Hooks, M. A., C. S. Wade, and W. J. Millikan, Jr. 1991. Muromonab CD-3: a review of its pharmacology, pharmacokinetics, and clinical use in transplantation. *Pharmacotherapy* 11: 26–37.
22. Casale, T. B., I. L. Bernstein, W. W. Busse, C. F. LaForce, D. G. Tinkelman, R. R. Stoltz, R. J. Dockhorn, J. Reimann, J. Q. Su, R. B. Fick, Jr., and D. C. Adelman. 1997. Use of an anti-IgE humanized monoclonal antibody in ragweed-induced allergic rhinitis. *J. Allergy Clin. Immunol.* 100: 110–121.
23. Subramanian, K. N., L. E. Weisman, T. Rhodes, R. Ariagno, P. J. Sánchez, J. Steichen, L. B. Givner, T. L. Jennings, F. H. Top, Jr., D. Carlin, and E. Connor. 1998. Safety, tolerance and pharmacokinetics of a humanized monoclonal antibody to respiratory syncytial virus in premature infants and infants with bronchopulmonary dysplasia; MEDI-493 Study Group. *Pediatr. Infect. Dis. J.* 17: 110–115.
24. Maloney, D. G., A. J. Grillo-López, C. A. White, D. Bodkin, R. J. Schilder, J. A. Neidhart, N. Janakiraman, K. A. Foon, T. M. Liles, B. K. Dallaire, et al. 1997. IDEC-C2B8 (Rituximab) anti-CD20 monoclonal antibody therapy in patients with relapsed low-grade non-Hodgkin's lymphoma. *Blood* 90: 2188–2195.
25. Tokuda, Y., T. Watanabe, Y. Omuro, M. Ando, N. Katsumata, A. Okumura, M. Ohta, H. Fujii, Y. Sasaki, T. Niwa, and T. Tajima. 1999. Dose escalation and pharmacokinetic study of a humanized anti-HER2 monoclonal antibody in patients with HER2/neu-overexpressing metastatic breast cancer. *Br. J. Cancer* 81: 1419–1425.
26. van de Winkel, J. G., and C. L. Anderson. 1991. Biology of human immunoglobulin G Fc receptors. *J. Leukoc. Biol.* 49: 511–524.
27. Wenig, K., L. Chatwell, U. von Pawel-Rammingen, L. Björck, R. Huber, and P. Sondermann. 2004. Structure of the streptococcal endopeptidase IdeS, a cysteine proteinase with strict specificity for IgG. *Proc. Natl. Acad. Sci. USA* 101: 17371–17376.
28. Davis, P. M., R. Abraham, L. Xu, S. G. Nadler, and S. J. Suchard. 2007. Abatacept binds to the Fc receptor CD64 but does not mediate complement-dependent cytotoxicity or antibody-dependent cellular cytotoxicity. *J. Rheumatol.* 34: 2204–2210.
29. Presta, L. G. 2008. Molecular engineering and design of therapeutic antibodies. *Curr. Opin. Immunol.* 20: 460–470.
30. Scallon, B., A. Cai, N. Solowski, A. Rosenberg, X. Y. Song, D. Shealy, and C. Wagner. 2002. Binding and functional comparisons of two types of tumor necrosis factor antagonists. *J. Pharmacol. Exp. Ther.* 301: 418–426.
31. Martin, W. L., and P. J. Bjorkman. 1999. Characterization of the 2:1 complex between the class I MHC-related Fc receptor and its Fc ligand in solution. *Biochemistry* 38: 12639–12647.
32. Gurbaxani, B. M., and S. L. Morrison. 2006. Development of new models for the analysis of Fc-FcRn interactions. *Mol. Immunol.* 43: 1379–1389.
33. Martin, W. L., A. P. West, Jr., L. Gan, and P. J. Bjorkman. 2001. Crystal structure at 2.8 A of an FcRn/heterodimeric Fc complex: mechanism of pH-dependent binding. *Mol. Cell* 7: 867–877.
34. Osborne, R. 2009. Fresh from the biologic pipeline. *Nat. Biotechnol.* 27: 222–225.
35. Cines, D. B., U. Yasothan, and P. Kirkpatrick. 2008. Romiplostim. *Nat. Rev. Drug Discov.* 7: 887–888.
36. Pan, H., K. Chen, L. Chu, F. Kinderman, I. Apostol, and G. Huang. 2009. Methionine oxidation in human IgG2 Fc decreases binding affinities to protein A and FcRn. *Protein Sci.* 18: 424–433.
37. Chaudhury, C., S. Mehnaz, J. M. Robinson, W. L. Hayton, D. K. Pearl, D. C. Roopenian, and C. L. Anderson. 2003. The major histocompatibility complex-related Fc receptor for IgG (FcRn) binds albumin and prolongs its lifespan. *J. Exp. Med.* 197: 315–322.
38. Chaudhury, C., C. L. Brooks, D. C. Carter, J. M. Robinson, and C. L. Anderson. 2006. Albumin binding to FcRn: distinct from the FcRn-IgG interaction. *Biochemistry* 45: 4983–4990.
39. Steinhauser, I., B. Spänkuch, K. Strebhardt, and K. Langer. 2006. Trastuzumab-modified nanoparticles: optimisation of preparation and uptake in cancer cells. *Biomaterials* 27: 4975–4983.
40. Wuang, S. C., K. G. Neoh, E. T. Kang, D. W. Pack, and D. E. Leckband. 2008. HER-2-mediated endocytosis of magnetic nanospheres and the implications in cell targeting and particle magnetization. *Biomaterials* 29: 2270–2279.
41. Tabrizi, M. A., C. M. Tseng, and L. K. Roskos. 2006. Elimination mechanisms of therapeutic monoclonal antibodies. *Drug Discov. Today* 11: 81–88.
42. Kuester, K., and C. Kloft. 2006. Pharmacokinetics of monoclonal antibodies. In *Pharmacokinetics and Pharmacodynamics of Biotech Drugs*. B. Meibohm, ed. Wiley-VCH Verlag, Weinheim, Germany, p. 45–91.